Augmin complex activity fine-tunes dendrite morphology through non-centrosomal microtubule nucleation *in vivo*

Yun Zhang[1,*,§], Hsin-Ho Sung[2,*], Anna B. Ziegler[1,*,‡,¶], Ying-Chieh Wu[2,*], Ricardo Viais[3], Carlos Sánchez-Huertas[3,**], Lukas Kilo[§§], Fikret-Gürkan Agrican[1], Ying-Ju Cheng[2], Kousuke Mouri[4,‡‡], Tadashi Uemura[4,5], Jens Lüders[3], Cheng-Ting Chien[2,‡], Gaia Tavosanis[1,6,§§]

[1]German center for neurodegenerative diseases (DZNE), Dynamics of Neuronal Circuits Group, Venusberg Campus 1 Building 99, 53127 Bonn
[2]Institute of Molecular Biology, Academia Sinica, 11529 Taipei, Taiwan
[3]Institute for Research in Biomedicine (IRB Barcelona), The Barcelona Institute of Science and Technology, Baldiri Reixac 10, 08028, Barcelona, Spain
[4]Graduate School of Biostudies, Kyoto University, Kyoto 606-8501, Japan
[5]Center for Living Systems Information Science, Kyoto University, Japan
[6]LIMES Institute, University of Bonn, 53115 Bonn, Germany

[*]Equal contribution
[‡]Authors for correspondence:
[§]Present address: The Brain Cognition and Brain Disease Institute (BCBDI), Shenzhen Institute of Advanced Technology, Chinese Academy of Sciences, Shenzhen 518055, China
[¶]Present address: University of Muenster, Institute for Neuro- and Behavioral Biology, Röntgenstraße 19, 48149 Muenster, Germany
[**]Present address: Instituto de Neurociencias, Consejo Superior de Investigaciones Científicas-Universidad Miguel Hernández (CSIC-UMH), Alicante, Spain
[‡‡]Present address: The Jackson Laboratory, Bar Harbor, ME 04609, USA
[§§]Present address: RWTH Aachen University, Lehrstuhl für Entwicklungsbiologie, Worringerweg 3, 52056 Aachen, Germany

Keywords: Neuronal Dendrites, Microtubules, Augmin, HAUS, γ-tubulin, *Drosophila* c4da neurons, Hippocampal neurons.

Summary statement

During neuronal development augmin stimulates microtubule nucleation and is required in vivo in Drosophila c4da neurons to fine-tune their complex dendrite morphology.

Abstract

During development neurons achieve a stereotyped neuron type-specific morphology, which relies on dynamic support by microtubules (MTs). An important player is augmin which binds to existing MT filaments and recruits the γ-Tubulin Ring Complex (γ-TuRC), to form branched MTs. In cultured neurons, augmin is important for neurite formation. However, little is known about the role of augmin during neurite formation in vivo. Here, we have revisited the role of mammalian augmin in culture and then turned towards the class four *Drosophila* dendritic arborization (c4da) neurons. We show that MT density is maintained through augmin in cooperation with the γ-TuRC *in vivo*. Mutant c4da neurons show a reduction of newly emerging higher-order dendritic branches and in turn also a reduced number of their characteristic space-filling higher-order branchlets. Taken together, our data reveal a cooperative function of the augmin complex with the γ-TuRC in forming enough MTs needed for the appropriate differentiation of morphologically complex dendrites *in vivo*.

Introduction

Neurons are highly polarized cells displaying a high morphological variability (Neukirchen and Bradke 2011; Hill et al. 2012; Lefebvre et al. 2015). To a large extent, this variation is caused by the diversity of the neuron type-specific dendritic trees (Jan and Jan 2010; Lefebvre et al. 2015; Tavosanis 2021). The branched dendrites receive and integrate input information – therefore, their complexity relates to the number and distribution of their inputs. Neuron type-specific dendritic morphologies are established during development and any changes leading to errors during this process can impact the function of the mature neuron (Ziegler et al. 2017; Ferreira Castro et al. 2020). The cytoskeleton is essential for dendrite elaboration. While actin is involved in the dynamics that support dendrite branching and elaboration, microtubules (MTs) are thought to promote the stabilization of branch subsets (Delandre et al. 2016; Nanda et al. 2020; Kilo et al. 2021). MTs are polarized polymers nucleating from microtubule organizing centers (MTOCs) (González et al. 1998; Sanchez and Feldman 2017; Wu and Akhmanova 2017). A key component of MTOCs is γ-tubulin (γ-Tub), which assembles with the γ-Tub complex proteins (GCPs) into the γ-Tub Ring Complex (γ-TuRC). In *Drosophila* the GCPs include Grip75, Grip84, Grip91, Grip128, and Grip163, in mammals they are termed GCP 1-6 (Fig. 1)

(Gunawardane et al. 2000; Thawani and Petry 2021). In proliferating cells γ-TuRCs concentrate at the centrosome which functions as major MTOC (González et al. 1998). However, during differentiation, centrosomes of rodent and fly neurons gradually lose γ-tubulin and, concurrently, MTOC activity, while γ-Tub localization is shifted to the cytoplasm, suggesting that the role of the centrosome is taken over by acentrosomal MT nucleation mechanisms in post-mitotic neurons (Leask et al. 1997; Stiess et al. 2010; Yonezawa et al. 2015; Sánchez-Huertas et al. 2016; Vinopal et al. 2023) . In fact, reducing this non-centrosomal γ-Tub fraction led to decreased MT polymerization in later stage neurons leading to reduced neurite number and length (Sánchez-Huertas et al. 2016; Cunha-Ferreira et al. 2018). Multiple studies thus focused on clarifying the mechanisms behind γ-Tub-dependent cytosolic MT polymerization in post-mitotic neurons. In the soma of differentiated *Drosophila* dendritic arborization (da) neurons, fluorescently labeled γ-Tub localizes predominantly to the Golgi stacks and Golgi outposts in proximal dendrites were suggested to gain MTOC activity (Ori-McKenney et al. 2012; Wu and Akhmanova 2017; Mukherjee et al. 2020). However, follow up studies indicated that γ-Tub-dependent MT nucleation in dendrites can also work independently of an interaction with Golgi outposts (Nguyen et al. 2014; Yalgin et al. 2015; Mukherjee et al. 2020). Along this line, very recently, endosomes at the growing tips of dendrites were additionally described as MT nucleation sites in *C.elegans* and *Drosophila* dendrites (Liang et al. 2020; Weiner et al. 2020).

As an alternative to organelle-based MTOC activity, MTs can also form from pre-existing MT filaments. In such a scenario, short MT fragments could act as seeds that provide free plus-ends for MT elongation. These MT seeds may be created through severing of existing filaments and minus-end stabilization (Wood et al. 2006; Yu et al. 2008; Stewart et al. 2012; Jiang et al. 2014; Buijs et al. 2021). This model is supported by observations made in fruit fly c4da neurons mutant for the MT-severing ATPases Spastin and Katanin 60L1 which show reduced dendritic complexity (Stewart et al. 2012; Buijs et al. 2021). Another possibility is that MTs are nucleated as branches from pre-existing MTs by augmin. This hetero-octameric complex was firstly shown to recruit γ-TuRCs to the lattice of a pre-existing mother MT filament and thereby trigger new MT growth within the mitotic spindle in dividing *Drosophila* Schneider 2 cells (Goshima et al. 2008). Augmin and its mammalian homologue, the Homologous to Augmin Subunit (HAUS) complex, consist of eight-subunits, termed

Dgt2-7, Wac, and Msd-1 in *Drosophila* and HAUS 1-8 in mammals (Fig. 1A) (Wu et al. 2008; Lawo et al. 2009; Uehara et al. 2009; Hsia et al. 2014). Recent structural studies have shown that augmin is composed of a V-shaped head made of Msd1, Dgt4, Dgt6, and Dgt7 (also called Msd5), which refer to HAUS2, HAUS8, HAUS6, and HAUS7 in mammals, and a tail made of Dgt2, Dgt3, Dgt5, and Wac, which refer to HAUS4, HAUS3, HAUS5, and HAUS1 in mammals (Hsia et al. 2014; Gabel et al. 2022). All eight subunits are required for augmin to fulfill its function. However, augmin subunit HAUS8/Dgt4 is primarily responsible for binding to the MT lattice while γ-TuRC is recruited through an interaction between Dgt6 (HAUS6 in mammals) and Grip71 (Nedd1 in mammals) to set a starting point for a newly nucleating MT branch (Wu et al. 2008; Lawo et al. 2009; Uehara et al. 2009; Hsia et al. 2014; Song et al. 2018). *In vitro,* purified augmin alone did not change MT nucleation dynamics, while branched MT density was significantly enhanced upon the cooperation of augmin and purified γ-TuRC complexes, indicating that augmin strictly requires the γ-TuRC for MT-based nucleation (Alfaro-Aco et al. 2020; Tariq et al. 2020).

A recent set of studies revealed the importance of augmin function in dendrite and axon development of rodent hippocampal neurons (Sánchez-Huertas et al. 2016; Cunha-Ferreira et al. 2018; Viais et al. 2021). In detail, during neocortical development, augmin is at first necessary for initial neuronal polarization and radial migration in embryonic mouse neurons *in vivo* (Cunha-Ferreira et al. 2018). At a later developmental stage, knockdown of augmin complex members or of γ-Tub in cultured hippocampal neurons decreased neurite number, length, and complexity (Sánchez-Huertas et al. 2016; Cunha-Ferreira et al. 2018). In fact, reduced expression of augmin complex members phenocopied the morphological simplification observed in γ-Tub knockdown neurons (Sánchez-Huertas et al. 2016; Cunha-Ferreira et al. 2018). This phenotype could be rescued by simultaneous overexpression of HAUS subunits (Cunha-Ferreira et al. 2018). Augmin and γ-TuRC interact biochemically, as HAUS6 can be co-immunoprecipitated with the γ-TuRC member GCP3 in lysates from cultured hippocampal cells *in vitro* (Sánchez-Huertas et al. 2016). Additionally, Green fluorescent protein (GFP)-tagged HAUS2 co-localized to approximately 45% with mCherry-tagged γ-TuRC complex member GCP2 at 10 days *in vitro* (DIV10). Finally, p-Syn-tdTomato-MACF18, a MT plus-end marker, labeled MT plus-end tips emerging from GFP-HAUS2 labeled clusters indicating that MTs can be nucleated in an augmin-dependent manner

(Cunha-Ferreira et al. 2018). In consequence, loss of augmin subunits led to a decreased number of polymerized MTs (Sánchez-Huertas et al. 2016; Cunha-Ferreira et al. 2018). Taken together, these studies showed that augmin interacts with the γ-TuRC to nucleate MTs in neurites and support neurite morphogenesis.

In addition to this role in dendrite and axonal growth, loss of augmin also affected MT polarity in axons. MTs in axons are oriented with their fast-growing plus-end pointing away from the cell body and thus polymerize in the anterograde direction. By contrast, while very early generated dendrites are marked by high levels of plus-end-out MTs, during later differentiation minus-end-out MTs are gradually added until a mixed polarity is obtained in vertebrate dendrites and an almost uniform minus-end-out polarity is obtained in invertebrate dendrites (Stone et al. 2008; Hill et al. 2012; Yau et al. 2016; Feng et al. 2019). Therefore, in invertebrate dendrites MTs are mostly polymerizing in retrograde direction (towards the cell body). Multiple mechanisms have already been identified that control MT polarity in axons and dendrites (recently reviewed by (Rolls 2022)). In cultured neurons knocking down augmin subunits increased the fraction of retrograde-polymerizing MTs in axons leading to axons with MTs of mixed polarity. This led to the hypothesis that augmin-mediated MT nucleation is used to produce new MTs based on the polarity of the pre-existing MTs (Sánchez-Huertas et al. 2016; Cunha-Ferreira et al. 2018). On the contrary, MT polarity was shown to be unaffected by loss of augmin function in dendrites of cultured neurons (Cunha-Ferreira et al. 2018). Lastly, stage E13.5 or E17.5 embryos of a conditional mouse HAUS6 knock out (KO) mutant displayed massive defects in brain development. For example, the radial thickness of the neuronal layer within the thalamus was reduced by 90%. However, those defects were linked to mitotic errors as well as p53-dependent apoptosis, and no effects of HAUS6 loss on neurons after E17.5 were examined (Viais et al. 2021).

Taken together, these studies point towards an important role of augmin in γ-TuRC dependent MT nucleation and morphogenesis in neurons. However, while knockdown of augmin subunits was shown to impair dendritic complexity in mature neurons in culture, its role in dendrite formation during early developmental stages and how it affects dendrite development *in vivo* has not been explored.

Larval *Drosophila* dendritic arborization (da) neurons have been extensively used for *in vivo* studies on the neurodevelopmental role of cytoskeletal regulators (Jan and Jan 2010). The da sensory neurons extend their dendrites under the

animals' almost transparent cuticle. Da neurons are classified into four classes based on the complexity of their dendritic trees and their distinct functions, with c1da proprioceptive neurons displaying a simple dendritic tree and c4da neurons, that respond to nociceptive stimuli, displaying a highly elaborate arbor (Grueber et al. 2002; Hughes and Thomas 2007; Hwang et al. 2007).

In this study, we first revisited the role of the augmin in cultured mouse hippocampal neurons and found that it is important for developmental growth of early-stage dendrites. Knockdown of two different augmin subunits did not alter MT polarity but reduced dendritic microtubule growth and density. To determine how branching nucleation may affect dendritic development *in vivo*, we next analyzed the function of the *Drosophila* homologue of the augmin complex in supporting dendrite arborization in the c4da neurons. Here, in agreement with the findings in cultured rodent neurons, we first provide evidence for reduced MT density along dendritic projections in augmin mutant neurons compared to controls. Using *in vivo* time lapse imaging, we show that this loss in MT density correlates with a reduced number of newly forming dendritic higher order branches, which are the morphological hallmarks of c4da neurons (Grueber et al. 2002). Lastly, genetic interaction of augmin and the γ-TuRC suggests a common role in this neurodevelopmental process *in vivo.* Taken together, using neuronal culture and *in vivo* models, our data provide evidence for a coordinated action of augmin and the γ-TuRC to support non-centrosomal MT nucleation in developing dendrites, which is required for the formation of higher order dendritic branches in morphologically complex neurons. Together with previous work, our results establish augmin as a crucial factor for non-centrosomal microtubule nucleation across all neuronal compartments and developmental stages to drive neuronal morphogenesis.

Results

Depletion of HAUS1 or HAUS7 complex members impairs dendrite and axonal length.

During differentiation, embryonic cortical neurons initially develop a trailing process that later becomes the axon and a leading edge that becomes the apical dendrite (Polleux and Snider 2010). An increased fraction of Mouse cortical neurons, in which the augmin member HAUS6 is depleted, is lacking these processes at

embryonic stage E14.5. Also, differentiated late stage mouse hippocampal neurons in culture (DIV12), in which HAUS2 or HAUS6 have been knocked down, have reduced dendritic complexity (Cunha-Ferreira et al. 2018). Complementing this work, we now tested the role of augmin in neurite outgrowth at very early stages by depleting two other subunits (HAUS1 or HAUS7) via RNA interference (RNAi) in cultured mouse hippocampal neurons from DIV1 to DIV4 (Fig. 1B and C). Efficient knockdown of augmin by HAUS1 or HAUS7 shRNA was demonstrated by Western blot in our previous study (Sánchez-Huertas et al. 2016). We measured reduced dendritic spanning reflected by a lower number of crossings of Scholl intersections in depleted neurons (Fig. 1C). Additionally, total dendritic length was reduced (Fig. 1D). Axon length in depleted neurons was also shorter (Fig. 1E). Thus, augmin is involved in dendrite growth not only in more mature neurons (DIV12), but also during very early differentiation stages (DIV4 and below).

Augmin was shown to sustain adequate levels of polymerized tubulin as the dendrites of HAUS6 depleted neurons at DIV12 display decreased levels of □-Tub and Acetyl-□-Tub (Cunha-Ferreira et al. 2018). We now analyzed □-Tub and Acetyl-□-Tub in developing dendrites of HAUS1- or HAUS7-depleted neurons at the earlier DIV4 stage and found them to be decreased (Fig. 2A-C). Together with previous work (Sánchez-Huertas et al. 2016; Cunha-Ferreira et al. 2018), our results suggest that augmin is involved in both establishment and maintenance of a dense MT array in dendrites of cultured neurons.

The lack of augmin function was previously shown to affect not only MT density but also MT polarity as developing axons of cultured HAUS1 and HAUS7 depleted mouse neurons at DIV4 contained MTs of reverse polarity compared to the almost exclusive plus-end-out orientation in control axons (Sánchez-Huertas et al. 2016). In contrast, no augmin-dependent impact on MT polarity was found in dendrites of later stage neurons (DIV12) (Sánchez-Huertas et al. 2016; Cunha-Ferreira et al. 2018). We have carefully revisited this finding by knocking down HAUS1 or HAUS7 between 1DIV to 5DIV and using EB3-Tomato, a MT plus-end binding protein that allows tracing the direction of MT growth (Stepanova et al. 2003). No effect of HAUS1 or HAUS7 depletion could be observed in proximal dendrites, but we found a decreased total number of EB3-labeled comets in the distal segments of dendrites. However, MT polarity in distal segments was not changed (Fig. 2D-G, Fig. S1). Taken together, in agreement with previous findings in more mature neurons

(Sánchez-Huertas et al. 2016; Cunha-Ferreira et al. 2018), our data show that augmin is important for nucleating MTs in developing dendrites, impacting on MT density and stability, but not on MT polarity.

Dgt5 affects MT density in c4da neurons

We next aimed at investigating whether depleting *Drosophila* augmin would also affect MT density in dendrites *in vivo* using c4da neurons as a cellular model. To test whether these express augmin we used the *PBac{IT.GAL4}dgt5*$^{0899\text{-}G4}$ allele which carries a Gal4 inserted into the *dgt5* 5´UTR and hence could represent a reporter for *dgt5* expression. *Dgt5-Gal4* mediated expression of *UAS-CD4::RFP* colocalized with the c4da neuronal marker *ppk-CD4::GFP* (Fig. 3A). An additional neuronal cell type within the larval peripheral nervous system (PNS) was labeled which is most likely a c3da neuron (Fig. 3A). To examine the MT levels in c4da neurons with reduced augmin complex function, we firstly labeled identified da neuronal dendrites by *109(2)80-Gal4* driven expression of membrane-tethered *UAS-mCD8GFP* and co-labeled these cells using a monoclonal anti-Futsch antibody. Futsch is the fly homologue of Microtubule-associated protein 1B (MAP1B). It binds MTs and its labeling intensity, detected by immunohistochemistry, can be used as a proxy for MT density (Fig. 3B) (Hummel et al. 2000). Anti-Futsch immunolabeling gradually decreased along the length of control c4da neuronal dendrites. Simultaneous expression of a *dgt5* RNAi construct, which efficiently knocked down *dgt5* expression levels (Fig. S2A, B), reduced anti-Futsch immunolabeling along the length of the dendrites (Fig. 3C and D). We verified this reduction using an alternative MT marker (Jupiter::mCherry) (Karpova et al. 2006) (Fig. S3 A-C) and studying γ-Tub::GFP localization in c4da neurons (Fig. S3D-F). Note that the *ppk-Gal4* driver used for this experiment is not fully specific for c4da neurons and is additionally weakly expressed in a c3da neuron (Fig. S3D). However, the c4da neuronal dendrites could be distinguished from the c3da neuronal ones by the more specific *ppk::tdTomato* expression. γ-Tub::GFP labeling could be observed in the main branches and the fine higher order branchlets of control c4da neurons, while this signal was absent or very weak in the higher order branchlets upon *dgt5* knockdown. In contrast to this effect on MT distribution, actin localization revealed by the actin reporter LifeAct-GFP (Riedl et al. 2008) was not modified within these branchlets after RNAi-mediated knockdown of *dgt5* (Fig. S3G/H).

Finally, we quantified MT densities in electron microscopy (EM) images obtained from control da neurons and after *dgt5* knockdown (Fig. 3E-G). In our EM images, we could not assay the exact position of the cut dendrite within its neuron. Upon *dgt5* knockdown, MT density was clearly reduced in thinner dendrites which most likely corresponds to the more distal dendrite fragments (Fig. 3F/G). To address if this correlates with a reduced amount of newly polymerizing MTs, we imaged EB1::GFP comets in c4da terminal dendrites and found a reduction upon *dgt5* depletion (Fig. 3H). In rodent HAUS mutant neurons in culture the uniform MT polarity is shifted towards a mixed one (Sánchez-Huertas et al. 2016; Cunha-Ferreira et al. 2018). To test the polarity of MTs in axons *in vivo* we additionally assayed EB1::GFP comets in c4da neuronal axons. We did not find a significant reduction of EB1::GFP comets but confirmed that in axons loss of augmin leads to a mixed MT polarity. Interestingly the uniformly retrograde MT polarity in distal dendrites was not affected (Fig. S4). Taken together, these results show that augmin is involved in maintaining a sufficient dendritic MT density *in vivo* and to define the polarity of MTs in neuronal axons.

Augmin subunits control dendrite elaboration of *Drosophila* c4da neurons *in vivo.*

We next tested whether loss of augmin affects dendritic morphology of the complex c4da neurons. To do so we depleted one by one the eight individual augmin subunits via RNAi in c4da neurons using *ppk-Gal4* and found a significant reduction in the number of c4da neuron dendritic branches in all cases (Fig. 4A and B). To further confirm the RNAi knock-down result, $dgt5^{LE10}$ and $dgt6^{19A}$ mutant alleles were generated by using P-element imprecise excision. The obtained the $dgt5^{LE10}$ allele is an almost full deletion of the coding region and homozygous mutant $dgt5^{LE10}$ embryos do not develop into larvae. We also tried to obtain a null mutant *dgt6* allele by mobilization of the {GSV}GS11802 P-element (originally described in Goshima et al., 2006) and thereby created the $dgt6^{19A}$ allele that displayed reduced gene expression. Dgt5 could not be detected in extracts from $dgt5^{LE10}$ homozygous mutant embryos, supporting that $dgt5^{LE10}$ is a null mutant, and Dgt6 protein levels were strongly reduced in $dgt6^{19A}$ 3rd instar mutant larvae extracts, indicating that $dgt6^{19A}$ is a strong hypomorph (Fig. S2C). In contrast, Dgt5 and Dgt6 proteins could be detected in extracts from mutant animals, carrying *krüppel-Gal4* to drive *UAS-dgt5* or *UAS-dgt6* expression in the embryonic ectoderm (Golembo et al. 1996), respectively (Fig. S2C).

We next tested whether loss of Dgt5 or Dgt6 function affects dendritic morphology *in vivo* by imaging the dendrites of c4da neurons in immobilized late-stage larvae (wandering LIII stage) using confocal microscopy. Since *dgt5*^{LE10} homozygous animals did not survive to the larval stages, homozygous mutant single c4da neuron clones were obtained using the MARCM (Mosaic analysis with a repressible cell marker) technique (Lee and Luo 2001). *dgt5*^{LE10} mutant c4da neurons displayed a reduced number of dendrite terminal branches correlating with overall simplified dendrite morphology. A similar simplification of the dendritic arbor was also observed in the c4da neurons of *dgt6*^{19A} homozygous mutant larvae at the wandering LIII stage (Fig. 5A,B). To confirm the specificity and to address cell-autonomy, we re-expressed wild type *dgt5* or *dgt6* selectively in the *dgt5*^{LE10} or the *dgt6*^{19A} mutant c4da neurons, respectively, which largely rescued dendrite morphology (Fig. 5A,B). Augmin depletion affected the MT density in da neurons more in higher order distal dendrites (Fig. 3B-G). We therefore separately counted the number of primary, secondary, tertiary and higher order dendritic branches in *dgt5*^{LE10} or *dgt6*^{19A} mutant neurons. This analysis showed that higher order dendritic branches, including the terminal branches, were reduced in *dgt5*^{LE10} or *dgt6*^{19A} mutant neurons (Fig. 5C). During development, especially the terminal branches are dynamically growing and retracting (Stürner et al. 2022). To investigate whether loss of augmin function acts on the formation and stabilization of newly emerging branches *in vivo*, we captured the elaboration of c4da neuron dendrites by time lapse imaging of second instar larvae (~ 72 h AEL), in which c4da terminal branchlets are highly dynamic. We found a reduction in the number of newly forming branches in homozygous mutant *dgt6*^{19A} c4da neurons (Fig. 5D).

C4da neurons display the most complex dendrites among da neurons. Their main branches are enriched in MTs while the higher order branches are enriched in actin (Nithianandam and Chien 2018; Nanda et al. 2020). On the contrary, the simple dendrite branches of c1da neurons all display only a clear microtubule signal (Nanda et al. 2020). We therefore tested whether augmin function is specifically needed for establishing a complex dendritic morphology, such as in c4da neurons, or if neurons with simpler dendritic morphology may also require augmin. To do so, we analyzed the dendrites of *dgt5* mutant c1da MARCM clones. However, in *dgt5*^{LE10} null-mutant c1da neurons, dendrite branch numbers and the overall dendrite length were not affected (Fig. 5 E-G). We additionally tested c1da neurons in which *dgt5* or *dgt6*

expression levels were knocked down via RNAi using the c1da neuron-specific *IG1-Gal4* driver line (Fig. S5). Likewise, dendritic morphology was unaffected in these mutants. Taken together, our data indicate that augmin is cell-autonomously required for proper dendrite formation of complex c4da neurons *in vivo.* Since augmin acts on terminal dendrite formation we speculated that it may also be localized at the more distal dendritic regions. Dgt6 immunostaining using anti-Dgt6 antibodies was only detectable in c4da neuronal cell bodies and high background signal prevented analyzing potential localization in the dendrites (Fig. S6A). We additionally generated an *UAS-eGFP::dgt6* transgene and expressed it in c4da neurons. The patchy dendritic eGFP::Dgt6 signal that did not localize to any specific dendritic compartments such as branch points (Fig. S6B). Also, the overexpression of this construct significantly reduced dendrite branching which suggests that this fusion protein acts as a dominant negative allele (Fig. S6 C-E).

Augmin complex regulates terminal branch dynamics in c4da neurons in cooperation with the γ-TuRC.

Augmin is reported to recruit the γ-TuRC to pre-existing MT filaments (Song et al. 2018). We thus tested how loss of γ-TuRC components γTub23C or Grip71 might affect dendrite morphology in c4da neurons in comparison to augmin mutant c4da neurons and found that their absence decreased dendritic complexity (Fig. 6A and B) to a similar extent as the loss of augmin subunits (Fig. 5A and B). In both cases, dendritic complexity defects could be rescued by re-expression of γTub23C or Grip71 in the respective mutant background in c4da neurons, demonstrating the cell-autonomous function of these subunits on dendrite morphology (Fig. 6A and B).

We next used *in vivo* time lapse imaging to test if, similarly to $dgt6^{19A}$ mutant neurons, new branch formation is affected in neurons with an impaired γ-TuRC. Although to a milder extent, a lack of γTub23C and Grip71 phenocopied the loss of the augmin subunit Dgt6 (Fig. 5D) by causing a reduction of newly forming branches (Fig. 6C). To test for a potential cooperation between these two complexes, we investigated terminal branch numbers in trans-heterozygous combinations of augmin mutants $dgt5^{LE10}$ or $dgt6^{19A}$ with mutations affecting γTuRC components. While heterozygous single mutants of augmin or γTuRC subunits did not display a measurable reduction of dendrite endpoints in c4da neurons, trans-heterozygous combinations of $γtub23C^{A15-2}$ with either $dgt5^{LE10}$ or $dgt6^{19A}$ mutants or of the

grip71^{120} allele in combination with *dgt6*^{19A} yielded branch reduction (Fig. 6D and E) supporting the view that the two protein complexes cooperate to support dendrite formation. Note that the trans-heterozygous combination of *grip71*^{120} and *dtg5*^{LE10} did not lead to a measurable effect compared to the single heterozygous mutant neurons. Taken together, these results strongly suggest that the Augmin complex works together with the γ-TuRC to regulate the dynamics of terminal dendrites in c4da neurons of *Drosophila* larvae.

Discussion

Augmin ensures robust MT density in dendrites to drive dendritic development in cultured neurons and *in vivo*

During development neurons acquire very diverse and cell-type specific morphologies. This morphological diversity depends on the expression of specific combinations of cytoskeletal regulators that temporally and locally promote a specific branching pattern (Nanda et al. 2020; Stürner et al. 2022). While few neuron type-specific actin regulators were uncovered which determine type-specific morphological characteristics, less is known about neuron type-specific MT nucleation mechanism (Coles and Bradke 2015; Kilo et al. 2021; Tavosanis 2021; Stürner et al. 2022). Multiple lines of evidence together indicated a cooperation of the γ-TuRC and augmin promoting neurite elaboration in cultured hippocampal neurons. In this context, augmin was suggested to nucleate MTs of the same polarity as the mother MT filament and thereby to increase MT density in a polarity-controlled manner (Sánchez-Huertas et al. 2016; Cunha-Ferreira et al. 2018; Viais et al. 2021).

In particular, depletion of γ-Tub or the augmin subunits HAUS1 or HAUS7 in cultured primary rodent hippocampal neurons at 4DIV led to a reduction of total □-tubulin levels and subsequently impaired axon specification and outgrowth (Sánchez-Huertas et al. 2016). In more mature neurons (11/12DIV), augmin clusters were distributed along axons and dendrites suggesting that augmin may regulate local MT nucleation events also in dendrites. Indeed, at this stage HAUS2 or HAUS6 knockdown impaired not only axon but also dendrite outgrowth. Furthermore, this loss of axonal and dendritic growth and complexity correlated with a reduction in MT density (Cunha-Ferreira et al. 2018). In the present study, we extended those findings

to the dendrite organization of primary hippocampal neuron cultures at very early stages (DIV4). Our data show that even at these early stages of differentiation depletion of HAUS1 or HAUS7, impaired dendritic growth and branching by decreasing MT levels while leaving MT polarity unaffected.

We next examined whether augmin's role in controlling MT density in dendrites is conserved and relevant *in vivo*. By fluorescently labeling the dendritic MTs of c4da neurons of *Drosophila* larvae, we found diminished levels of MT markers in the distal dendrite segments of augmin deficient c4da neuron. Additionally, the density of microtubules in thin distal dendrites of da neurons was diminished, as observed in electron microscopy preparations. Together, these data suggest that augmin complex-mediated nucleation is involved in establishing and maintaining dense MT arrays in specific dendritic compartments *in vivo*.

Loss of augmin does not alter MT polarity in dendrites

In the rodent hippocampal neurons in culture as well as in *Drosophila* c4da neurons *in vivo*, absence of augmin affects MT polarity in the axon but not in the dendrites- a display of striking conservation (Fig. 2G, Fig S4). To explain why loss of augmin function does not alter MT polarity in dendrites, we note that the augmin γ-TuRC complex nucleates microtubule branches at shallow angles (Kamasaki et al. 2013; Petry et al. 2013; Verma and Maresca 2019) and thus branch polarity is determined by the polarity of the mother microtubule. This suggests that augmin does not define *de novo* the orientation of MTs, but that it consolidates their existing orientation. The control of MT orientation in axons may not be very strict; alternatively, a tight control on MT orientation may be temporally restricted to the very early stages of axon formation and elongation. In either case, loss of augmin in axons may lead to some randomized nucleation events without polarity control, which would explain the observed incorrectly oriented (minus-end out) MTs (Sánchez-Huertas et al. 2016; Cunha-Ferreira et al. 2018). By contrast, the mechanisms that define the specific MT orientation in dendrites of different types of neurons might be stricter or these mechanisms could be maintained active also in differentiated neurons. Loss of augmin may therefore not lead to polarity defects in dendrites, but merely to a reduction in MT density.

Loss of augmin function affects the formation of higher order branches in c4da neurons in cooperation with the γ-TuRC

Using multiple approaches, we showed that the loss of augmin and γ-TuRC affects the formation of higher order dendritic branches in c4da neurons. Here, loss of augmin function within c4da neurons (Fig. 5A and B) resulted in a similar dendrite simplification phenotype as the loss of γ-TuRC activity (Fig. 6 A and B). A cooperative function of augmin with the γ-TuRC was further supported by the genetic interaction displayed by subunits of the two complexes (Fig. 6 D and E). We therefore suggest that the cooperation with augmin may be an important prerequisite for the γ-TuRC to be recruited and nucleate MTs in distal dendrites to promote formation of higher-order dendrite branches. In line with this suggestion augmin mutant c1da neurons, that have morphologically simple dendrites lacking higher-order branchlets, do not show overall morphological changes (Fig. S5).

This agrees with previous studies showing no overall changes in c1da dendrite morphology when the function of γ-Tub or of the augmin subunit Wac was impaired (Nguyen et al. 2014; Yalgin et al. 2015; Weiner et al. 2020). Interestingly, in c1da neurons the γ-TuRC recruiting factor Centrosomin (Cnn) displays an antagonistic role to Wac (Yalgin et al. 2015). While anterograde polymerizing MTs promote outgrowth and stabilization of nascent dendritic branches (Ori-McKenney et al. 2012; Yalgin et al. 2015), Cnn promotes retrograde MT nucleation and growth from Golgi outposts to restrict dendrite branching in c1da neurons (Yalgin et al. 2015). In c1da neurons, thus, anterograde polymerisation promoted by Augmin/Wac could support the stabilization of newly formed dendritic branches. The interplay between these two different MT nucleation mechanisms may be a way to regulate dendrite branching by fine-tuning MT polymerization event numbers and MT polarity in c1da neurons (Yalgin et al. 2015; Wilkes and Moore 2020). It will be interesting to test whether this interplay might be involved also in the distinctive arbour of c4da neurons.

The neuron type-specific variations in phenotype expression between c1da and c4da neurons may be explained by the developmental differences between those two neuronal classes. The main branches of the c1da neuronal dendritic tree are set during the embryonic stage and afterwards scale with the growth of the animal with only few new dendritic branchlets being added (Ferreira Castro et al. 2020; Palavalli et al. 2021). In contrast, c4da neurons are continuously gaining

dendrite complexity until the late LIII stage (Baltruschat et al. 2020). This temporal distinction might lead to the availability for c1da neurons of maternally supplied augmin during the phase in which dendrites are established. In contrast, at the time in which higher order branches are formed in c4da neurons, the augmin level in the mutants might be already neglectable (Vastenhouw et al. 2019). A more intriguing hypothesis would be that different mechanisms are in place in c1da and in c4da neurons to control dendrite branching. Specifically in case of c4da neurons, these would require appropriate MT density guaranteed by augmin function.

Nevertheless, it is important to note that c4da neurons are still capable of forming their type-specific dendritic tree – with just less characteristic space-filling higher order branchlets. This indicates that the development of higher order branches in c4da neurons does only partially rely on the augmin complex. Indeed, parallel mechanisms of MT nucleation are employed to nucleate MTs and to support dendritic branch formation (Wilkes and Moore 2020). Early endosomes house Wnt signaling proteins which recruit γ-Tub to dendritic branch points (Weiner et al. 2020). Furthermore, MTs can be generated even independently of γ-Tub by severing of existing filaments through Katanin and Spastin and transport of short MT fragments into the neurites via motor-based sliding where they act as local MT nucleation seeds (Yu et al. 2005; Wood et al. 2006; Yu et al. 2008; Stewart et al. 2012). Therefore, all so far described MT nucleation mechanisms may, to a given extent, functionally compensate for the loss of each other. In parallel, *de novo* branchlet formation also strongly depends on actin-nucleation (Stürner et al. 2022). Nonetheless, we found no change in localization and abundance of LifeAct-GFP levels in terminal dendrites (Fig. S3G,H). This suggested that, in addition to the above-mentioned MT nucleation mechanisms, actin nucleation could in part compensate for the loss of augmin-dependent MT nucleation and help to maintain a large fraction of terminal dendrites in augmin mutant neurons. How the actin-based and the MT-supported mechanisms might interact in this context is unclear.

Lastly, MTs are not only providing mechanical support to a cell but simultaneously also function as tracks for MT-based motors to traffic material and machinery needed for neurite branching and growth (Kapitein and Hoogenraad 2015; Schelski and Bradke 2017; Santos et al. 2020; Schelski and Bradke 2022). For instance, in axons reduced γ-Tub levels were shown to diminish the amount and motility of mitochondria in axons (Sánchez-Huertas et al. 2016). However, to what

level transport is affected in augmin deficient dendrites still needs to be investigated.

In summary, our study establishes the requirement of neuronal augmin function for γ-TuRC mediated MT nucleation in dendrite development *in vitro* and *in vivo* and, using c4da neurons as a morphologically complex *in vivo* model, revealed a specific role for augmin- γ-TuRC in elaborating the formation of higher-order dendritic branches.

Material and Methods

Statistical analysis:

Data were analyzed with GraphPad Prism 7 and represent mean ± SD unless otherwise stated. In box-and-whisker plots whiskers represent lower and upper quartile. Asterisks are as follows: ns: $p > 0.05$; *: $p \leq 0.05$; **: $p \leq 0.01$; ***: $p \leq 0.001$; ****: $p \leq 0.0001$.

Mice generation and maintenance

To obtain embryonic brain tissue, pregnant 6-weeks-old female mice (Mus musculus; strain OF1) were purchased from Janvier Laboratories and maintained at the animal facilities of the Barcelona Science Park (PCB), in strict accordance with the Spanish and European Union regulations. Protocols were approved by the Animal Care and Use Committee of the PCB (IACUC; CEEA-PCB) in accordance with applicable legislation (Real Decreto 53/2013).

Hippocampal cell culture

At e17.5-e18.5 days of gestation, females were euthanized by cervical dislocation and embryos were sacrificed by decapitation. Brain tissue was dissected on 10 cm dishes placed on ice containing cold Hank's solution (0.14 M NaCl, 1 mM $CaCl_2$, 0.4 mM $MgSO_4 \cdot 7H_2O$, 0.5 mM $MgCl_2 \cdot 6H_2O$, 0.3 mM $Na_2HPO_4 \cdot 2H_2O$, 0.4 mM KH_2PO_4, 6 mM D-Glucose, 0.4 mM $NaHCO_3$, pH 7.4 – all reagents from Merck/Sigma). Isolated hippocampi were treated with 0.25% trypsin (Life Technologies) and DNAse (Roche) for 15 minutes at 37°C and dissociated into single cells by gentle pipetting. Neuron

density in suspension was calculated by counting cells in a Neubauer chamber. Neurons were seeded on glass coverslips or plastic plates pre-coated with 0.1 mg/ml Poly-D-lysine (Sigma) in Borate Buffer pH 8.5 at 6.6 x 104 cells per cm2 for time-lapse microscopy experiments and at 1 × 104 cells per cm^2 for immunofluorescence experiments in plating medium (DMEM containing 10% fetal bovine serum (FBS) and penicillin/streptomycin 100 IU/ml and 100 µg/ml, respectively). After 2h, Plating medium was replaced by Maintenance Medium, consisting of Neurobasal medium supplemented with 2% B27, penicillin/streptomycin (100 IU/ml and 100 µg/ml, respectively), 0.6% Glucose and Glutamax (all reagents from Life Technologies). Neurons were maintained at 37°C in a humidified atmosphere containing 5% CO_2.

Lentivirus production and transduction using HEK293T cells

Lentivirus was generated using the LentiLox3.7 system. HEK293T cells were cultured in DMEM containing 10% FBS and penicillin/streptomycin (100 IU/ml and 100 µg/ml, respectively) and kept at 37°C in a humidified atmosphere containing 5% CO_2. HEK293T cells were co-transfected with a pLKO.1 plasmid containing the desired shRNA, and the viral package and envelope plasmids, by using calcium phosphate. 72 hours later, lentivirus particles were concentrated by ultracentrifugation at 27000 rpm for 2 hours at 4°C. Virus particles were resuspended in ice-cold PBS and aliquoted and stored at −80°C. Virus titration was performed by evaluating a GFP-carrying virus produced in parallel with pLKO.1 expressing virus. Infectivity was assayed for GFP-carrying virus by infecting HEK293T cells with serial dilutions of the concentrated lentivirus and sorting of GFP-positive cells by FACS 72 hours after infection. Neurons were infected at 1 DIV at multiplicity of infection 6. The complete medium was replaced with fresh Maintenance medium 16–18 hours after infection.

Immunofluorescence staining of cultured neurons

In vitro cultured neurons were fixed at 4 DIV using 4% PFA diluted in PHEM buffer (60 mM Pipes, 25 mM Hepes pH 7.4, 5 mM EGTA, 1 mM $MgCl_2$) supplemented with 4% sucrose, 0.25% glutaraldehyde and 0.1% Triton X-100 (Sigma-Aldrich). Fixed cells were washed with PBS and permeabilized with 0.25% Triton X-100 in PBS for 5 minutes, blocked for 1 hour with 4% bovine serum albumin (BSA, Sigma-Aldrich) diluted in PBS and incubated overnight at 4◦C with primary antibodies (anti-α-tubulin

(DM1A, Sigma, dilution 1:2,000) and anti-Acetylated- α-tubulin (6-11B-1, Sigma, dilution 1:50,000), in blocking solution in a wet chamber. Secondary Antibodies conjugated with Alexa488 or Alexa568 were obtained from Life Technologies and used at 1:250.

Microscopy

To analyze α-tubulin / acetylated-α-tubulin levels, and dendritic and axonal length in HAUS1 and HAUS7 depleted neurons single-plane images were acquired with an Orca AG camera (Hamamatsu) coupled to Leica DMI6000B microscope. For analysis of α-tubulin / acetylated-α-tubulin levels, a 40x objective was used. To assemble mosaics of complete axons/dendritic arbors 20x and 10x objectives were used and complete mosaics were reconstructed using the Las X software (Leica).

Microtubule polarity assay

Hippocampal cultures were plated in 0.1mg/ml Poly-D-lysine coated glass-bottom dishes (MatTek), transduced with virus expressing shRNA at 1 DIV and transfected with EB3-Tomato reporter expressing plasmid at 3DIV. EB3-comets of randomly transfected neurons were imaged 24 hours later using an Olympus IX81 microscope equipped with Yokogawa CSU-X1 spinning disc and a temperature-controlled CO_2 incubation chamber. The proximal dendrite region was defined as ~20 µm from the soma and distal dendritic region was defined as ~20 µm away from the dendritic tip. Image stacks were acquired with 100x/1.4 OIL immersion objective and an iXon EMCCD Andor DU-897 camera, using iQ2 software. Fluorescent images with a pixel size of 0.14 µm were taken at intervals of 1 second for 150 seconds. Multiple planes were imaged with a step size of 0.2 µm. Z-stacks were performed by using ImageJ software (NIH).

EB-1 number and polarity assay

For visualizing polymerizing MTs we used *ppk-EB-1-GFP* (Arthur et al. 2015). C4da neurites were identified using *ppk*-mCD4-tdTomato. *ppk-EB1-GFP*, ppk-*mCD4-tdTomato*, and *ppk-Gal4* carrying flies (generously provided by S. Rumpf) were crossed to *UAS-Dicer2; UAS-dgt5 RNAi* to induce a knockdown. Feeding L3 larvae

were mounted in halocarbon oil and immobilized in a specially designed imaging chamber (Dimitrova et al. 2008; Baltruschat et al. 2020). Image acquisition for the EB-1 kymographs was done using a Leica SP8 confocal microscope with a resonant scan head to achieve the needed temporal resolution. Short image stacks of individual c4da neuron dendrite branches and axons respectively were recorded with a frequency of one stack per every 2 seconds for 5 minutes using a 63x N.A. 1.4 oil immersion objective. Image stacks were processed and analyzed using ImageJ software (National Institutes of Health, Bethesda, 596 Maryland, USA, http://rsb.info.nih.gov/ij/). Motion artifacts were corrected using ImageJ 3D drift correction plugin as well as the Image stabilizer plugin (K. Li, "The image stabilizer plugin for ImageJ," http://www.cs.cmu.edu/~kangli/code/ImageStabilizer.html, February 2008). Statistical data analysis was done using Graphpad Prism (Version 9.1.1.(255)). EB1 comets in kymographs were analyzed also by a blinded lab member that was not involved in generating the raw data.

Image analysis

To measure α-Tub and acetyl-α-Tub signal intensities were measured in images acquired with constant exposure settings and background-subtracted intensities were normalized to the average intensity of the control.

Whole axon and dendritic lengths were measured using the NeuronJ macro (ImageJ software). Sholl analysis was performed using the Sholl analysis plugin as described before (Ferreira et al. 2014) using binary versions of the dendrite tracings generated with the NeuronJ plugin.

Axonal and dendritic EB3-comet analysis was performed using the kymograph macro (ImageJ software), with lines drawn on the trajectories of comets (Ezquerra et al. 2020).

Genetics and fly husbandry

Fly stocks and crosses were reared at 25°C on a standard fly medium unless otherwise stated. Generation of dgt619A: *dgt6{GSV}GS11802* P-element mutant males were crossed to *yw; Pin/ Cyo; Dr Δ{2-3}/ TM6, Ubx* (Bloomington Stock Nr. 5908). *dgt6{GSV}GS11802 / Dr Δ{2-3}* males of the F1 generation were crossed to a

third chromosome balancer line. A white eye phenotype in males of the F2 generation indicated single events of a Δ{2-3} dependent P-element removal and thus the putative generation of a new dgt6 allele trough imprecise P-element immobilization. Stable lines were created by balancing of the third chromosome of single white eyed males over TM6b. Each individual line was tested trough PCR and western blot for deletion of the *dgt6* coding region and *dgt619A* was used for further analysis. Sequencing of the $dgt6^{19A}$ genomic locus revealed that the protein coding sequence was not affected. However, the mobilization removed the UAS binding sites, which all GSV P-elements contain, and which in our experimental setup would have led to an unwanted Gal4-mediated overexpression of *dgt6*. Generation of $dgt5^{LE10}$: *w;* $dgt5^{EP2492}$ P-element mutant males were crossed to *yw; Pin/ Cyo; Dr Δ{2-3}/ TM6, Ubx* (Bloomington Stock Nr. 5908). $Dgt5^{EP2492}$ */ Dr Δ{2-3}* males of the F1 generation were crossed to a second chromosome balancer line. Stable lines were created by balancing of the second chromosome of single white eyed males over CyO. Each individual line was tested trough PCR for deletion of the *dgt5* coding region (GCCATCAGGTTGTCCAGCAATTG & CCAACTCATCTTCGGAGTCCTC) and $dgt5^{LE10}$ was used for further analysis. $\gamma tub23C^{P1}$ was kindly provided by C. Gonzalez (Barcelona, Spain) (Sunkel et al. 1995), $\gamma tub23C^{A15\text{-}2}$ (Vázquez et al. 2008) was obtained from the Bloomington stock center (Nr. 7042), g*rip120* (Reschen et al. 2012) was a kind gift from Jordan W. Raff (Oxford, UK), *UAS-γtub23C::GFP* was kindly provided by M. Rolls (Nguyen et al. 2014).

RNAi lines used: Stock Nr. 31729 obtained from the Bloomington Stock Center and the following strains were obtained from the VDRC stock center (Vienna, Austria): 103980 (UAS-dgt3 RNAi); 34901(UAS-dgt4 RNAi); 26911 (UAS-dgt5 RNAi); 16352 (UAS-dgt6 RNAi); 50460 (UAS-msd1 RNAi); 21713 (UAS-msd5 RNAi); 104962 (UAS-wac RNAi), ppk-gal4 driven expression of UAS-lacZ was used as a control. The following UAS and gal4 lines used in this study were obtained from the Bloomington Stock Center: 77584

(*w1118; PBac{IT.GAL4}dgt50899-G4/CyO*), 58800 (*y1 w*; P{GAL4-Kr.C}10o/TM3, Sb1*), 8768 (*y1 w*; P{GawB}109(2)80, P{UAS-mCD8::GFP.L}LL5*); 8746 (*y1 w*; P{GawB}477, P{UAS-mCD8::GFP.L}LL5*); 26259 (*w[*]; Pin[1]/CyO; P{GawB}221*); 55851 (w^{*}*; P{GAL4-da.G32}UH1,* Sb^{1}*/TM6B,* Tb^{1}); 32078 and 32079 (*ppk-Gal4*on 2nd and 3rd chromosome). *UAS-lacZ* and *UAS-mCD8::GFP* 3955 (2nd chromosome), 3956 (3rd chromosome); 5131 (2nd chromosome), 5130 (3rd

chromosome). *UAS-CD4dtTomato* was a kind gift from Y.N. Jan (Han et al. 2011),*UAS-Jupiter::mcherry* was a gift from C.Doe (Cabernard and Doe 2009) and □*Tub23C*^{PI} was kindly provided by C. Gonzalez (Sunkel et al. 1995). *UAS-LifeAct::GFP* was obtained from the Bloomington stock center (Nr.57326).

Molecular cloning and plasmids

The target sequence for depletion of mouse HAUS7 (sh HAUS7: CCAGATGACCAGGATCTTCTA) and HAUS1 (sh HAUS1: GCTGAACTTACCAAGAAAGTA) were cloned for expression as shRNAs into plKO.1 plasmids. A pLKO.1 plasmid expressing a scrambled sequence (CAACAAGATGAAGAGCACCAA) was used as control. All these pLKO.1 plasmids with shRNA constructs were obtained as bacteria clones from a library of the IRB Barcelona Functional Genomics facility (as a partnership with Sigma-Aldrich RNAi program). The reporter plasmid EB3-Tomato was a generous gift of Anne Straube (University of Warwick, UK).

The following Drosophila cDNA clones were obtained from the Drosophila Genomics Resource Center LD47477 (dgt5), LD14121 (dgt6), RE05579 (grip71) and used for the PCR amplification of the coding region using the following primers: TTAAGAATTCATGAAATGTGCC & GATCTCTAGATCATTCTAACAG (dgt5); CCGGAATTCATGGATCGGACCATAATTGCAC & CTAGTCTAGACTAAAAGATAATATCCTTG (dgt6); TTCCTTTTTTGCGGCCGCATGCATGTT & CTAGTCTAGATTACTCTCCGCATGATT (grip71) (Eurofins MWG Operon). PCR amplicons were cloned using XbaI and EcoRI for dgt5, EcoRI and XbaI for dgt6, and NotI and XbaI for grip71 into p{UAST}attB (Bischof et al. 2007). The open reading frame of each construct was sequenced. Transgenic flies were generated by BestGene (Chino Hills, US) by PhiC31-mediated integration into landing sites attP 51D (2nd chromosome) or attP 86F (3rd chromosome).

The eGFP-Dgt6 expression vector was generated by PCR amplifying *dgt6* cDNA PCR from the *dgt6* cDNA containing vector (provided by Dr. Goshima (Nagoya University, Japan) using the following primers: dgt6L (GATCGGACCATAATTGCACCGTGGAAGGCC) and dgt6R(CTAAAAGATAATATCCTTGAGCACGCTATCGCT). The PCR product was then

cloned into the PCR8 vector (Invitrogen), and subsequently was subcloned into Gateway Vectors pTGW(DGRC 1075)for *GFP-dgt6* expression constructs by performing an LR recombination. The construct was microinjected into w^{1118};*Δ2-3* (BDSC 2534) fly embryos and positive transformants picked upon expression of *mini-white*.

RT-PCR

The knockdown efficiency for *dgt5 dgt6* and *msd1* mRNAs was tested using RT-PCR. *daugthterless (da)-Gal4* (Bloomington Stock Nr. 8641) was used for the expression (Wodarz et al. 1995) of UAS-dsRNA constructs. Total RNA was extracted from larvae using the RNAzol®RT kit (Molecular Research Center, Inc.) and mRNA was reverse transcribed using the ImProm-II™ Reverse Transcription System (Promega) followed by a standard PCR protocol. Primers used were TAA CAG AAT TTA AGA ACT GGG CCA CTA ATC and TT GTT CTT CAA CTC CTG GTC GTA GTT CTT (*dgt5*); AAC TTC CTG CTC GAG TTC GTG GGC TT and ATG GCC TCC TTG AGA CCG CAC AGA GAT (*dgt6*); TGG ACA AAA TGT TGG CGG GAA TGG CG and TT CTT CAT CTG GCC CAC GGT GTC GTA (*msd1*). Amplification of ribosomal protein L19 cDNA using the following primers TCT CTA AAG CTC CAG AAG AGG C and CGA TCT CGT TGA TTT CAT TGG GA served as internal control.

qRT-PCR

RNA was isolated from 10 third instar larvae using 350 µl lysis buffer using the RNeasy® Mini Kit (Qiagen) following the manufacturer's instructions. Reverse transcription was done using 700 ng RNA and the QuantiTect® Reverse Transcription Kit (Qiagen). qRT-PCR reaction was done using TaqMan® Probes (ThermoFisher Scientific) Dm01819973_g1 (Catalog #4351372) in a qTOWER³ Real-Time-Thermocycler (Analytik Jena).

Generation of MARCM cell clones

Homozygote *dgt5* mutant c4da neurons were generated using the MARCM technique (Lee and Luo 2001). To do so *dgt5LE10* was recombined with *FRT42D*. Next, *hsFLP, elav-Gal4 UAS-mCD8::GFP; FRT42D, tubGal80/Cyo* (gift from Takashi Suzuki) virgins were collected and crossed to *dgt5LE10, FRT42D/CyO-GFP* males. Females were allowed to lay eggs on apple agar plates for 2 hours at 25°C and the eggs were

allowed to develop for 3h. Embryos were heat shocked twice 45 min at 38°C in a water bath with a 30 min resting period at RT in between the heat-shock cycles. Plates were kept at 25°C until wandering 3rd instar larvae could be selected for imaging.

Western blot analysis

For Dgt5 detection 20 embryos and for Dgt6 detection five 3rd instar larvae were selected and grinded in 100 µl 2x Laemmli buffer + 1 M DTT. Probes were boiled for 5 at 95°C and protein separation by SDS-PAGE was done under standard conditions. Protein transfer to a nitrocellulose membrane was done using Trans-blot Turbo (Bio-Rad). The membrane was blocked with 5% milk powder in washing buffer (0.1% Tween in PBS) for 1 hour at RT and was incubated with first antibody in a 1:1000 dilution overnight at 4°C. α-Dgt5 was a kind gift from Dr. Goshima's lab (Goshima et al. 2008) and α-Dgt6 was provided by Dr. Somma's lab (Bucciarelli et al. 2009). The membrane was washed 3x 5min and detected using HRP-conjugated anti-rabbit IgGs and the ECL detection kit (all from GE Healthcare) in a Chemi-doc (Bio-Rad). Anti-Actin was obtained from DSHB Hybridoma (#JLA20).

Confocal imaging of da neurons and data analysis

Wandering 3rd instar larvae were embedded in 87%-90% glycerol and immobilized in between a glass slide and a cover slip. The dorsal c4da neuron (ddaC) of segment A4 or A5 was imaged using a Zeiss LSM780 or a LSM710 confocal microscope using a 40x NA 1.4 oil immersion objective. Maximum projection images and image adjustments were made using ImageJ (National Institutes of Health, Bethesda, Maryland, USA, http://rsb.info.nih.gov/ij/) and analyzed using the NeuronJ plug-in (Meijering, Jacob et al. 2004). All dendritic branches were traced and classified into four classes. The long dendrites emerging from the soma were defined as primary dendrite. Dendrites emerged from the primary dendrites were defined as secondary dendrites. Tertiary dendrites were defined as the dendrites emerged from the secondary dendrites and the rest were defined as higher order branches. Each branch was categorized and measured in length.

Dendritic anti-Futsch signal quantification

A 20 µm wide line was drawn along a labeled (*Gal4109(2)80 > UAS-mCD8::GFP*) c4da neuronal dendrite using the ROI manager in ImageJ. The line was straightened and subdivided into 20 bins starting at the soma and reaching out to the dendritic tip. Anti-Futsch labeling was converted to gray values, background signal intensity subtracted, and the average signal intensity calculated for each of the 20 bins. Signal intensity of each bin of a control, UAS-lacZ expressing, dendrites was compared to the corresponding area of dendrites, in which dgt5 has been knocked down by RNAi.

Time lapse imaging

Late 2nd instar larvae were mounted in halocarbon oil and immobilized in between a metal sieve and a cover slip. One branch of a c4da neuron was imaged under a confocal microscope (Zeiss780) using a 40x NA 1.4 oil immersion objective with an interval of 5 min for 30 min. Stack images were processed with ImageJ software (National Institutes of Health, Bethesda, Maryland, USA, http://rsb.info.nih.gov/ij/) and photoshop (Adobe) for maximum projections and modifications.

Tracings for each time point were generated using the NeuronJ plug-in (Meijering, Jacob et al. 2004). The overall number of terminal branches was used to normalize our data set and the amount of newly formed branches was given in % ((newly formed branches/total branches) x100). By definition, we counted a branch as “new” once it appeared for the first time within the 30-minute time frame.

Immunostaining

Open book preparations of wandering 3rd instar larvae were fixed in 4% formaldehyde with 0.3% triton X-100 for 20 min at RT. Tissues were washed 3 x 10 min with PBS + 0.3 % triton X-100 (PBST). Next, samples were incubated with mouse anti-Futsch (1:100, DSHB, Iowa City, US) primary antibody in PBST + 10% normal donkey serum (NDS) at 4°C overnight. Afterwards they were washed 4 x 10 min in PBT and incubated with a Cy5 conjugated anti-mouse secondary antibody (Jackson ImmunoResearch Laboratories) in PBST + 10% NDS overnight at 4°C. Preparations were washed 4 x10 min in PBT and mounted using PBS with 87.5% glycerol and 0.22 M 1,4-diaza-byciclo (2.2.2) octane (Dabco, SigmaCo). Confocal

stack images of ddaC neurons were obtained using a LSM710 (Zeiss) confocal microscope using a 20x objective.

Electron Microscopy

Sample preparation and detection were conducted as previously described (Tsai et al., 2012). Briefly, dissected larval body walls were fixed at room temperature (RT) for 30 min followed by 4 °C ON in modified Trump's fixative (0.1 M sodium cacodylate buffer, 1% glutaraldehyde, and 4% formaldehyde). They were washed 3 x 10 min in 0.1 M sodium cacodylate, postfixed for 30 min with 2% osmium tetroxide in 0.1 M sodium cacodylate buffer washed 3 x 10 min with 0.1 M sodium cacodylate buffer and 5 x 10 min with ddH2O. Specimens were incubated in 2% aqueous uranyl acetate for 20 min, dehydrated by a graded ethanol series, and set into Spurr's embedding medium. Thin sections (90 nm) were stained with uranyl acetate and lead citrate. Images were viewed on a Tecnai G2 Spirit TWIN electron microscope (FEI Company) and captured on a Gatan CCD camera (794.10.BP2 MultiScan). Transmission electron microscopy (TEM) data were quantified by MetaMorph V6.3r7 (Molecular Devices).

Acknowledgements

We thank Astrid Fleige, Regina Hube, and Rita Kerpen for technical assistance. The reporter plasmid EB3-Tomato was a generous gift of A. Straube (University of Warwick, UK). We thank C. Gonzalez, S. Rumpf, J. Raff, M. Rolls, YN Jan, C. Doe, T. Suzuki, the Bloomington Stock Center and the Vienna Stock Center for providing fly lines. We thank G. Goshima for α-Dgt5 and M.P. Somma for providing α-Dgt6 antibodies. We thank K. Doubkova and M. Davies for comments on the manuscript. We thank Dr. P. Conduit for discussing results prior to publication.

Competing interests

The authors declare no competing or financial interests.

Funding

This work was supported by a Deutsche Forschungsgemeinschaft grant (Teilprojekt, SPP 1464) to G.T.. C.-T. C. was supported by grants from National Science and Technology, Taiwan, and Academia Sinica, Taiwan. Work in the group of J.L. was supported by grants from the Ministerio de Ciencia, Innovación y Universidades with FEDER funds (BFU2015-69275-P, PGC2018-099562-B-I00, PID2021-127603NB-I00, RED2022-134792-T), grant 2021 SGR 01280 (L'Agència de Gestió d'Ajuts Universitaris i de Recerca, Generalitat de Catalunya) and IRB Barcelona intramural funds. R.V. was supported by a Severo Ochoa PhD fellowship (SVP-2014-068770; Ministerio de Ciencia, Innovación y Universidades). T.U. was supported by a Core Research for Evolutionary Science and Technology (CREST) grant from Japan Science and Technology Agency (JST) and a Research Grant in the Natural Sciences from Mitsubishi Foundation. K.M. was a recipient of a fellowship from the Japan Society for the Promotion of Science

References

Alfaro-Aco, R., Thawani, A. and Petry, S. 2020. Biochemical reconstitution of branching microtubule nucleation. *eLife* 9. doi: 10.7554/eLife.49797.

Arthur, A.L., Yang, S.Z., Abellaneda, A.M. and Wildonger, J. 2015. Dendrite arborization requires the dynein cofactor NudE. *Journal of Cell Science* 128(11), pp. 2191–2201. doi: 10.1242/jcs.170316.

Baltruschat, L., Tavosanis, G. and Cuntz, H. 2020. A developmental stretch-and-fill process that optimises dendritic wiring. *BioRxiv*. doi: 10.1101/2020.07.07.191064.

Bischof, J., Maeda, R.K., Hediger, M., Karch, F. and Basler, K. 2007. An optimized transgenesis system for Drosophila using germ-line-specific phiC31 integrases. *Proceedings of the National Academy of Sciences of the United States of America* 104(9), pp. 3312–3317. doi: 10.1073/pnas.0611511104.

Bucciarelli, E., Pellacani, C., Naim, V., Palena, A., Gatti, M. and Somma, M.P. 2009. Drosophila Dgt6 interacts with Ndc80, Msps/XMAP215, and gamma-tubulin to promote kinetochore-driven MT formation. *Current Biology* 19(21), pp. 1839–1845. doi: 10.1016/j.cub.2009.09.043.

Buijs, R.R. et al. 2021. WDR47 protects neuronal microtubule minus ends from katanin-mediated severing. *Cell reports* 36(2), p. 109371. doi: 10.1016/j.celrep.2021.109371.

Cabernard, C. and Doe, C.Q. 2009. Apical/basal spindle orientation is required for neuroblast homeostasis and neuronal differentiation in Drosophila. *Developmental Cell* 17(1), pp. 134–141. doi: 10.1016/j.devcel.2009.06.009.

Coles, C.H. and Bradke, F. 2015. Coordinating neuronal actin-microtubule dynamics. *Current Biology* 25(15), pp. R677-91. doi: 10.1016/j.cub.2015.06.020.

Cunha-Ferreira, I. et al. 2018. The HAUS Complex Is a Key Regulator of Non-centrosomal Microtubule Organization during Neuronal Development. *Cell reports* 24(4), pp. 791–800. doi: 10.1016/j.celrep.2018.06.093.

Delandre, C., Amikura, R. and Moore, A.W. 2016. Microtubule nucleation and organization in dendrites. *Cell Cycle* 15(13), pp. 1685–1692. doi: 10.1080/15384101.2016.1172158.

Dimitrova, S., Reissaus, A. and Tavosanis, G. 2008. Slit and Robo regulate dendrite branching and elongation of space-filling neurons in Drosophila. *Developmental Biology* 324(1), pp. 18–30. doi: 10.1016/j.ydbio.2008.08.028.

Ezquerra, A., Viais, R. and Lüders, J. 2020. Assaying Microtubule Nucleation. *Methods in Molecular Biology* 2101, pp. 163–178. doi: 10.1007/978-1-0716-0219-5_11.

Feng, C. et al. 2019. Patronin-mediated minus end growth is required for dendritic microtubule polarity. *The Journal of Cell Biology* 218(7), pp. 2309–2328. doi: 10.1083/jcb.201810155.

Ferreira Castro, A., Baltruschat, L., Stürner, T., Bahrami, A., Jedlicka, P., Tavosanis, G. and Cuntz, H. 2020. Achieving functional neuronal dendrite structure through sequential stochastic growth and retraction. *eLife* 9. doi: 10.7554/eLife.60920.

Ferreira, T.A. et al. 2014. Neuronal morphometry directly from bitmap images. *Nature Methods* 11(10), pp. 982–984. doi: 10.1038/nmeth.3125.

Gabel, C.A. et al. 2022. Molecular architecture of the augmin complex. *Nature Communications* 13(1), p. 5449. doi: 10.1038/s41467-022-33227-7.

Golembo, M., Raz, E. and Shilo, B.Z. 1996. The Drosophila embryonic midline is the site of Spitz processing, and induces activation of the EGF receptor in the ventral ectoderm. *Development* 122(11), pp. 3363–3370. doi: 10.1242/dev.122.11.3363.

González, C., Tavosanis, G. and Mollinari, C. 1998. Centrosomes and microtubule organisation during Drosophila development. *Journal of Cell Science* 111 (Pt 18), pp. 2697–2706. doi: 10.1242/jcs.111.18.2697.

Goshima, G., Mayer, M., Zhang, N., Stuurman, N. and Vale, R.D. 2008. Augmin: a protein complex required for centrosome-independent microtubule generation within the spindle. *The Journal of Cell Biology* 181(3), pp. 421–429. doi: 10.1083/jcb.200711053.

Grueber, W.B., Jan, L.Y. and Jan, Y.N. 2002. Tiling of the *Drosophila* epidermis by multidendritic sensory neurons. *Development* 129(12), pp. 2867–2878. doi: 10.1242/dev.129.12.2867.

Gunawardane, R.N., Martin, O.C., Cao, K., Zhang, L., Dej, K., Iwamatsu, A. and Zheng, Y. 2000. Characterization and reconstitution of Drosophila gamma-tubulin ring complex subunits. *The Journal of Cell Biology* 151(7), pp. 1513–1524. doi: 10.1083/jcb.151.7.1513.

Han, C., Jan, L.Y. and Jan, Y.-N. 2011. Enhancer-driven membrane markers for analysis of nonautonomous mechanisms reveal neuron-glia interactions in Drosophila. *Proceedings of the National Academy of Sciences of the United States of America* 108(23), pp. 9673–9678. doi: 10.1073/pnas.1106386108.

Hill, S.E., Parmar, M., Gheres, K.W., Guignet, M.A., Huang, Y., Jackson, F.R. and Rolls, M.M. 2012. Development of dendrite polarity in Drosophila neurons. *Neural Development* 7, p. 34. doi: 10.1186/1749-8104-7-34.

Hsia, K.-C. et al. 2014. Reconstitution of the augmin complex provides insights into its architecture and function. *Nature Cell Biology* 16(9), pp. 852–863. doi: 10.1038/ncb3030.

Hughes, C.L. and Thomas, J.B. 2007. A sensory feedback circuit coordinates muscle activity in Drosophila. *Molecular and Cellular Neurosciences* 35(2), pp. 383–396. doi: 10.1016/j.mcn.2007.04.001.

Hummel, T., Krukkert, K., Roos, J., Davis, G. and Klämbt, C. 2000. Drosophila Futsch/22C10 is a MAP1B-like protein required for dendritic and axonal development. *Neuron* 26(2), pp. 357–370. doi: 10.1016/s0896-6273(00)81169-1.

Hwang, R.Y., Zhong, L., Xu, Y., Johnson, T., Zhang, F., Deisseroth, K. and Tracey, W.D. 2007. Nociceptive neurons protect Drosophila larvae from parasitoid wasps. *Current Biology* 17(24), pp. 2105–2116. doi: 10.1016/j.cub.2007.11.029.

Jan, Y.-N. and Jan, L.Y. 2010. Branching out: mechanisms of dendritic arborization. *Nature Reviews. Neuroscience* 11(5), pp. 316–328. doi: 10.1038/nrn2836.

Jiang, K. et al. 2014. Microtubule minus-end stabilization by polymerization-driven CAMSAP deposition. *Developmental Cell* 28(3), pp. 295–309. doi: 10.1016/j.devcel.2014.01.001.

Kamasaki, T., O'Toole, E., Kita, S., Osumi, M., Usukura, J., McIntosh, J.R. and Goshima, G. 2013. Augmin-dependent microtubule nucleation at microtubule walls in the spindle. *The Journal of Cell Biology* 202(1), pp. 25–33. doi: 10.1083/jcb.201304031.

Kapitein, L.C. and Hoogenraad, C.C. 2015. Building the neuronal microtubule cytoskeleton. *Neuron* 87(3), pp. 492–506. doi: 10.1016/j.neuron.2015.05.046.

Karpova, N., Bobinnec, Y., Fouix, S., Huitorel, P. and Debec, A. 2006. Jupiter, a new Drosophila protein associated with microtubules. *Cell Motility and the Cytoskeleton* 63(5), pp. 301–312. doi: 10.1002/cm.20124.

Kilo, L., Stürner, T., Tavosanis, G. and Ziegler, A.B. 2021. Drosophila dendritic arborisation neurons: fantastic actin dynamics and where to find them. *Cells* 10(10). doi: 10.3390/cells10102777.

Lawo, S. et al. 2009. HAUS, the 8-subunit human Augmin complex, regulates centrosome and spindle integrity. *Current Biology* 19(10), pp. 816–826. doi: 10.1016/j.cub.2009.04.033.

Leask, A., Obrietan, K. and Stearns, T. 1997. Synaptically coupled central nervous system neurons lack centrosomal gamma-tubulin. *Neuroscience Letters* 229(1), pp. 17–20. doi: 10.1016/s0304-3940(97)00412-6.

Lee, T. and Luo, L. 2001. Mosaic analysis with a repressible cell marker (MARCM) for Drosophila neural development. *Trends in Neurosciences* 24(5), pp. 251–254. doi: 10.1016/s0166-2236(00)01791-4.

Lefebvre, J.L., Sanes, J.R. and Kay, J.N. 2015. Development of dendritic form and function. *Annual Review of Cell and Developmental Biology* 31, pp. 741–777. doi: 10.1146/annurev-cellbio-100913-013020.

Liang, X., Kokes, M., Fetter, R.D., Sallee, M.D., Moore, A.W., Feldman, J.L. and Shen, K. 2020. Growth cone-localized microtubule organizing center establishes microtubule orientation in dendrites. *eLife* 9. doi: 10.7554/eLife.56547.

Mukherjee, A., Brooks, P.S., Bernard, F., Guichet, A. and Conduit, P.T. 2020. Microtubules originate asymmetrically at the somatic golgi and are guided via Kinesin2 to maintain polarity within neurons. *eLife* 9. doi: 10.7554/eLife.58943.

Nanda, S., Bhattacharjee, S., Cox, D.N. and Ascoli, G.A. 2020. Distinct roles of microtubules and actin filaments in defining dendritic architecture. *SSRN Electronic Journal*. doi: 10.2139/ssrn.3614134.

Neukirchen, D. and Bradke, F. 2011. Neuronal polarization and the cytoskeleton. *Seminars in Cell & Developmental Biology* 22(8), pp. 825–833. doi: 10.1016/j.semcdb.2011.08.007.

Nguyen, M.M. et al. 2014. Γ-tubulin controls neuronal microtubule polarity independently of Golgi outposts. *Molecular Biology of the Cell* 25(13), pp. 2039–2050. doi: 10.1091/mbc.E13-09-0515.

Nithianandam, V. and Chien, C.-T. 2018. Actin blobs prefigure dendrite branching sites. *The Journal of Cell Biology* 217(10), pp. 3731–3746. doi: 10.1083/jcb.201711136.

Ori-McKenney, K.M., Jan, L.Y. and Jan, Y.-N. 2012. Golgi outposts shape dendrite morphology by functioning as sites of acentrosomal microtubule nucleation in neurons. *Neuron* 76(5), pp. 921–930. doi: 10.1016/j.neuron.2012.10.008.

Palavalli, A., Tizón-Escamilla, N., Rupprecht, J.-F. and Lecuit, T. 2021. Deterministic and stochastic rules of branching govern dendrite morphogenesis of sensory neurons. *Current Biology* 31(3), pp. 459-472.e4. doi: 10.1016/j.cub.2020.10.054.

Petry, S., Groen, A.C., Ishihara, K., Mitchison, T.J. and Vale, R.D. 2013. Branching microtubule nucleation in Xenopus egg extracts mediated by augmin and TPX2. *Cell* 152(4), pp. 768–777. doi: 10.1016/j.cell.2012.12.044.

Polleux, F. and Snider, W. 2010. Initiating and growing an axon. *Cold Spring Harbor Perspectives in Biology* 2(4), p. a001925. doi: 10.1101/cshperspect.a001925.

Reschen, R.F., Colombie, N., Wheatley, L., Dobbelaere, J., St Johnston, D., Ohkura, H. and Raff, J.W. 2012. Dgp71WD is required for the assembly of the acentrosomal Meiosis I spindle, and is not a general targeting factor for the γ-TuRC. *Biology open* 1(5), pp. 422–429. doi: 10.1242/bio.2012596.

Riedl, J. et al. 2008. Lifeact: a versatile marker to visualize F-actin. *Nature Methods* 5(7), pp. 605–607. doi: 10.1038/nmeth.1220.

Rolls, M.M. 2022. Principles of microtubule polarity in linear cells. *Developmental Biology* 483, pp. 112–117. doi: 10.1016/j.ydbio.2022.01.004.

Sánchez-Huertas, C., Freixo, F., Viais, R., Lacasa, C., Soriano, E. and Lüders, J. 2016. Non-centrosomal nucleation mediated by augmin organizes microtubules in post-mitotic neurons and controls axonal microtubule polarity. *Nature Communications* 7, p. 12187. doi: 10.1038/ncomms12187.

Sanchez, A.D. and Feldman, J.L. 2017. Microtubule-organizing centers: from the centrosome to non-centrosomal sites. *Current Opinion in Cell Biology* 44, pp. 93–101. doi: 10.1016/j.ceb.2016.09.003.

Santos, T.E., Schaffran, B., Broguière, N., Meyn, L., Zenobi-Wong, M. and Bradke, F. 2020. Axon growth of CNS neurons in three dimensions is amoeboid and independent of adhesions. *Cell reports* 32(3), p. 107907. doi: 10.1016/j.celrep.2020.107907.

Schelski, M. and Bradke, F. 2017. Neuronal polarization: From spatiotemporal signaling to cytoskeletal dynamics. *Molecular and Cellular Neurosciences* 84, pp. 11–28. doi: 10.1016/j.mcn.2017.03.008.

Schelski, M. and Bradke, F. 2022. Microtubule retrograde flow retains neuronal polarization in a fluctuating state. *Science Advances* 8(44), p. eabo2336. doi: 10.1126/sciadv.abo2336.

Song, J.-G., King, M.R., Zhang, R., Kadzik, R.S., Thawani, A. and Petry, S. 2018. Mechanism of how augmin directly targets the γ-tubulin ring complex to microtubules. *The Journal of Cell Biology* 217(7), pp. 2417–2428. doi: 10.1083/jcb.201711090.

Stepanova, T. et al. 2003. Visualization of microtubule growth in cultured neurons via the use of EB3-GFP (end-binding protein 3-green fluorescent protein). *The Journal of Neuroscience* 23(7), pp. 2655–2664.

Stewart, A., Tsubouchi, A., Rolls, M.M., Tracey, W.D. and Sherwood, N.T. 2012. Katanin p60-like1 promotes microtubule growth and terminal dendrite stability in the larval class IV sensory neurons of Drosophila. *The Journal of Neuroscience* 32(34), pp. 11631–11642. doi: 10.1523/JNEUROSCI.0729-12.2012.

Stiess, M. et al. 2010. Axon extension occurs independently of centrosomal microtubule nucleation. *Science* 327(5966), pp. 704–707. doi: 10.1126/science.1182179.

Stone, M.C., Roegiers, F. and Rolls, M.M. 2008. Microtubules have opposite orientation in axons and dendrites of Drosophila neurons. *Molecular Biology of the Cell* 19(10), pp. 4122–4129. doi: 10.1091/mbc.E07-10-1079.

Stürner, T., Ferreira Castro, A., Philipps, M., Cuntz, H. and Tavosanis, G. 2022. The branching code: A model of actin-driven dendrite arborization. *Cell reports* 39(4), p. 110746. doi: 10.1016/j.celrep.2022.110746.

Sunkel, C.E., Gomes, R., Sampaio, P., Perdigão, J. and González, C. 1995. Gamma-tubulin is required for the structure and function of the microtubule organizing centre in Drosophila neuroblasts. *The EMBO Journal* 14(1), pp. 28–36. doi: 10.1002/j.1460-2075.1995.tb06972.x.

Tariq, A., Green, L., Jeynes, J.C.G., Soeller, C. and Wakefield, J.G. 2020. In vitro reconstitution of branching microtubule nucleation. *eLife* 9. doi: 10.7554/eLife.49769.

Tavosanis, G. 2021. Dendrite enlightenment. *Current Opinion in Neurobiology* 69, pp. 222–230. doi: 10.1016/j.conb.2021.05.001.

Thawani, A. and Petry, S. 2021. Molecular insight into how γ-TuRC makes microtubules. *Journal of Cell Science* 134(14). doi: 10.1242/jcs.245464.

Uehara, R., Nozawa, R., Tomioka, A., Petry, S., Vale, R.D., Obuse, C. and Goshima, G. 2009. The augmin complex plays a critical role in spindle microtubule generation for mitotic progression and cytokinesis in human cells. *Proceedings of the National Academy of Sciences of the United States of America* 106(17), pp. 6998–7003. doi: 10.1073/pnas.0901587106.

Vastenhouw, N.L., Cao, W.X. and Lipshitz, H.D. 2019. The maternal-to-zygotic transition revisited. *Development* 146(11). doi: 10.1242/dev.161471.

Vázquez, M., Cooper, M.T., Zurita, M. and Kennison, J.A. 2008. gammaTub23C interacts genetically with brahma chromatin-remodeling complexes in Drosophila melanogaster. *Genetics* 180(2), pp. 835–843. doi: 10.1534/genetics.108.093492.

Verma, V. and Maresca, T.J. 2019. Direct observation of branching MT nucleation in living animal cells. *The Journal of Cell Biology* 218(9), pp. 2829–2840. doi: 10.1083/jcb.201904114.

Viais, R., Fariña-Mosquera, M., Villamor-Payà, M., Watanabe, S., Palenzuela, L., Lacasa, C. and Lüders, J. 2021. Augmin deficiency in neural stem cells causes p53-dependent apoptosis and aborts brain development. *eLife* 10. doi: 10.7554/eLife.67989.

Vinopal, S. et al. 2023. Centrosomal microtubule nucleation regulates radial migration of projection neurons independently of polarization in the developing brain. *Neuron* 111(8), pp. 1241-1263.e16. doi: 10.1016/j.neuron.2023.01.020.

Weiner, A.T. et al. 2020. Endosomal Wnt signaling proteins control microtubule nucleation in dendrites. *PLoS Biology* 18(3), p. e3000647. doi: 10.1371/journal.pbio.3000647.

Wilkes, O.R. and Moore, A.W. 2020. Distinct microtubule organizing center mechanisms combine to generate neuron polarity and arbor complexity. *Frontiers in Cellular Neuroscience* 14, p. 594199. doi: 10.3389/fncel.2020.594199.

Wodarz, A., Hinz, U., Engelbert, M. and Knust, E. 1995. Expression of crumbs confers apical character on plasma membrane domains of ectodermal epithelia of Drosophila. *Cell* 82(1), pp. 67–76. doi: 10.1016/0092-8674(95)90053-5.

Wood, J.D. et al. 2006. The microtubule-severing protein Spastin is essential for axon outgrowth in the zebrafish embryo. *Human Molecular Genetics* 15(18), pp. 2763–2771. doi: 10.1093/hmg/ddl212.

Wu, G., Lin, Y.-T., Wei, R., Chen, Y., Shan, Z. and Lee, W.-H. 2008. Hice1, a novel microtubule-associated protein required for maintenance of spindle integrity and chromosomal stability in human cells. *Molecular and Cellular Biology* 28(11), pp. 3652–3662. doi: 10.1128/MCB.01923-07.

Wu, J. and Akhmanova, A. 2017. Microtubule-Organizing Centers. *Annual Review of Cell and Developmental Biology* 33, pp. 51–75. doi: 10.1146/annurev-cellbio-100616-060615.

Yalgin, C. et al. 2015. Centrosomin represses dendrite branching by orienting microtubule nucleation. *Nature Neuroscience* 18(10), pp. 1437–1445. doi: 10.1038/nn.4099.

Yau, K.W., Schätzle, P., Tortosa, E., Pagès, S., Holtmaat, A., Kapitein, L.C. and Hoogenraad, C.C. 2016. Dendrites In Vitro and In Vivo Contain Microtubules of Opposite Polarity and Axon Formation Correlates with Uniform Plus-End-Out Microtubule Orientation. *The Journal of Neuroscience* 36(4), pp. 1071–1085. doi: 10.1523/JNEUROSCI.2430-15.2016.

Yonezawa, S., Shigematsu, M., Hirata, K. and Hayashi, K. 2015. Loss of γ-tubulin, GCP-WD/NEDD1 and CDK5RAP2 from the Centrosome of Neurons in Developing Mouse Cerebral and Cerebellar Cortex. *Acta histochemica et cytochemica* 48(5), pp. 145–152. doi: 10.1267/ahc.15023.

Yu, W., Qiang, L., Solowska, J.M., Karabay, A., Korulu, S. and Baas, P.W. 2008. The microtubule-severing proteins spastin and katanin participate differently in the formation of axonal branches. *Molecular Biology of the Cell* 19(4), pp. 1485–1498. doi: 10.1091/mbc.E07-09-0878.

Yu, W., Solowska, J.M., Qiang, L., Karabay, A., Baird, D. and Baas, P.W. 2005. Regulation of microtubule severing by katanin subunits during neuronal development. *The Journal of Neuroscience* 25(23), pp. 5573–5583. doi: 10.1523/JNEUROSCI.0834-05.2005.

Ziegler, A.B. et al. 2017. Cell-Autonomous Control of Neuronal Dendrite Expansion via the Fatty Acid Synthesis Regulator SREBP. *Cell reports* 21(12), pp. 3346–3353. doi: 10.1016/j.celrep.2017.11.069.

Figures

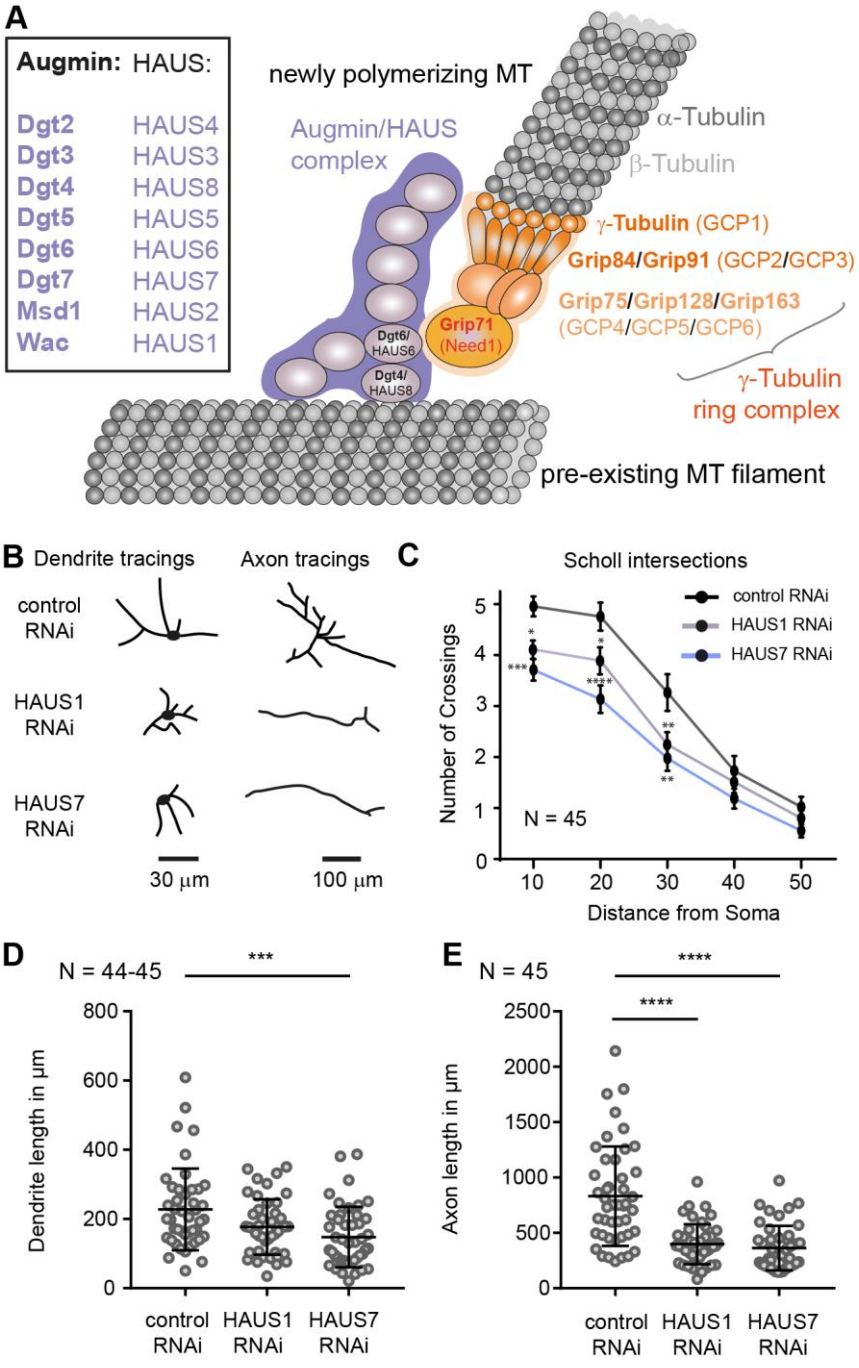

Fig. 1. Depletion of HAUS1 or HAUS7 complex members impairs dendrite and axon growth of hippocampal neurons. (A) Augmin consists of eight subunits (Dgt2-7, Wac and Msd-1 in *Drosophila* and HAUS1-8 in mammals) and interacts via Dgt4 (homologue of HAUS8) with pre-existing MT polymers. The γ-TuRC (orange) is recruited by an interaction between Dgt6 (homologue of HAUS6) and Grip71

(homologue of Need1). (See text for further details). **(B-E)** Primary hippocampal neuron cultures were transfected with shRNA and GFP expressing plasmids at 1DIV and fixed at 4DIV. **(B)** Representative tracings of cultured hippocampal neurons expressing a control plasmid (expressing a scrambled sequence), HAUS1 or HAUS7 RNAi constructs. **(C)** Depletion of HAUS1 or HAUS7 reduced neurite complexity measured by Scholl analysis. Data points represent mean with SEM. **(D,E)** Quantification of total dendritic and total axonal length of neurons as shown in B. Statistical test used in C, D and E: Kruskal-Wallis with Dunn´s multiple comparison test. N reflects number of neurons (biological replicates) unless otherwise stated.

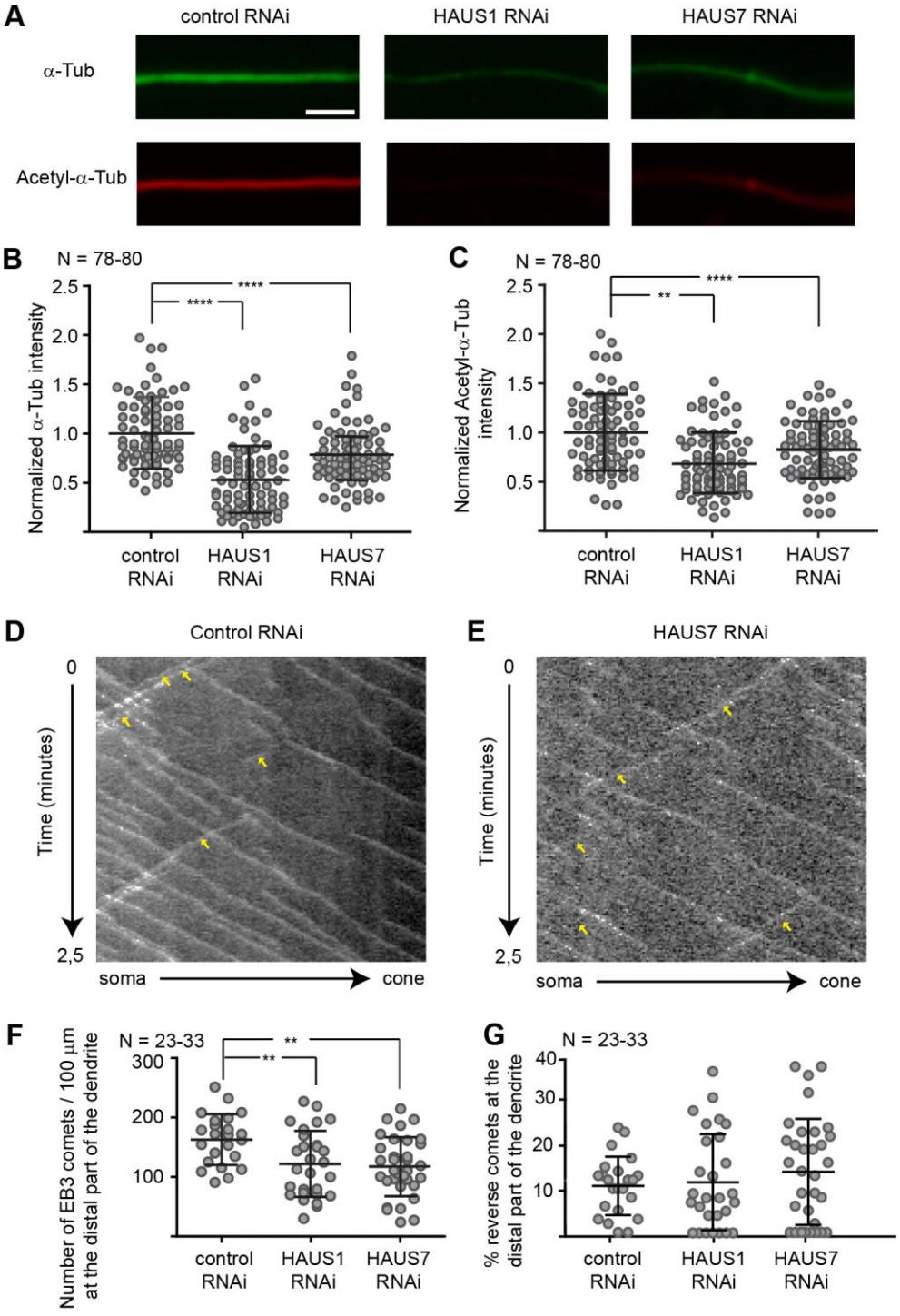

Fig. 2. HAUS1 or HAUS7 depletion reduces the amount of tubulin in dendrites but does not affect microtubule polarity.

(A-C) Primary hippocampal neuronal cultures were transfected with shRNA-expressing plasmids at 1DIV and fixed and stained using anti-□-Tub and anti-acetyl-□-Tub antibodies at 4DIV. **(A)** Representative images of □-Tub and acetyl-□-Tub labeling in dendrites (Scale bar = 10 µm). **(B,C)** Quantification of the normalized

mean signal intensity of □-Tub or acetyl-□-Tub in dendrites. **(D-G)** Primary hippocampal neuron cultures were co-transfected at 3DIV with HAUS1 or HAUS7 shRNA constructs and an EB3::tomato expression construct and imaged at 5DIV. **(D,E)** Representative kymographs of time-lapse recordings of EB3-comets in control or HAUS7-depleted dendrites. Reverse comets are marked by arrowheads. Quantification of the number of EB3-positive comets in the distal **(F)** part of the dendrites and % of retrograde comets **(G)** from kymographs as in D, E. Statistical test used in B: Kruskal-Wallis followed by Dunn´s multiple comparison test, and C, F, and G: 1-Way-ANOVA followed by Dunnett´s multiple comparison test.

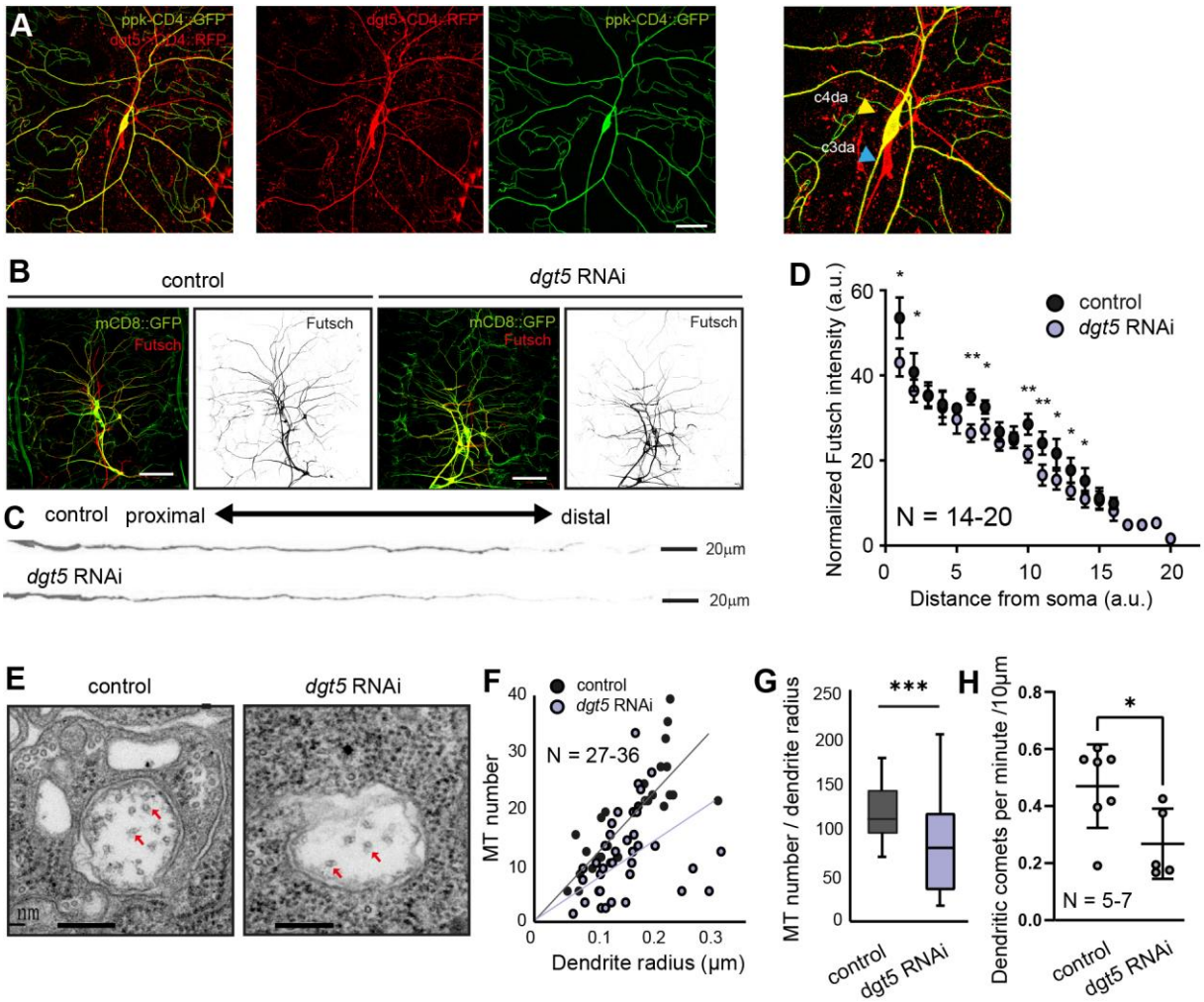

Fig. 3. Dgt5 supports appropriate MT density *in vivo* in da neurons(A) *dgt5-Gal4* mediated expression of *UAS-CD4::RFP* colocalizes with c4da marker ppk-CD4::GFP. Scale bar = 200 μm **(B-D)** Control or *UAS-dgt5* RNAi constructs were co-expressed with *UAS-mCD::8GFP* in da neurons using *109(2)80-Gal4*. Scale bar = 100 μm **(B)** Larval fillet preparations immunolabeled with anti-GFP antibodies (green; da neurons) and anti-Futsch antibodies (red; microtubules). Scale bar = 100 μm. **(C)** Individual dendrites were straightened by post-image processing and labeled with anti-Futsch antibodies. Scale bar = 20 μm **(D)** Distribution of anti-Futsch signal intensity along the relative length of dendrites. For quantification, every dendrite was divided to 20 segments and the average Futsch signal intensity normalized to mCD8::GFP intensity was calculated for each of the segments. **(E-G)** MT tubule number quantification in control and *dgt5* RNAi-depleted neurites **(E)** EM images show dendrite cross-sections of a control (left panel) and a *dgt5* RNAi-depleted neurite (right panel). MTs are indicated by yellow arrows. Scale bar = 200 nm. **(F)** MT

numbers divided by the dendrite radius were plotted against the dendrite radius. **(G)** MT number divided by dendrite radius. **(H)** Plus ends of growing microtubules are labeled by ppk-EB1::GFP and c4da neurites were identified using *ppk-Gal4* driven expression of *UAS-CD4::RFP*. EB1-comet number was measured in thin distal dendrites of control and *dgt5-RNAi* depleted cells. Data points represent mean with SEM. Statistics: unpaired student´s *t*-test.

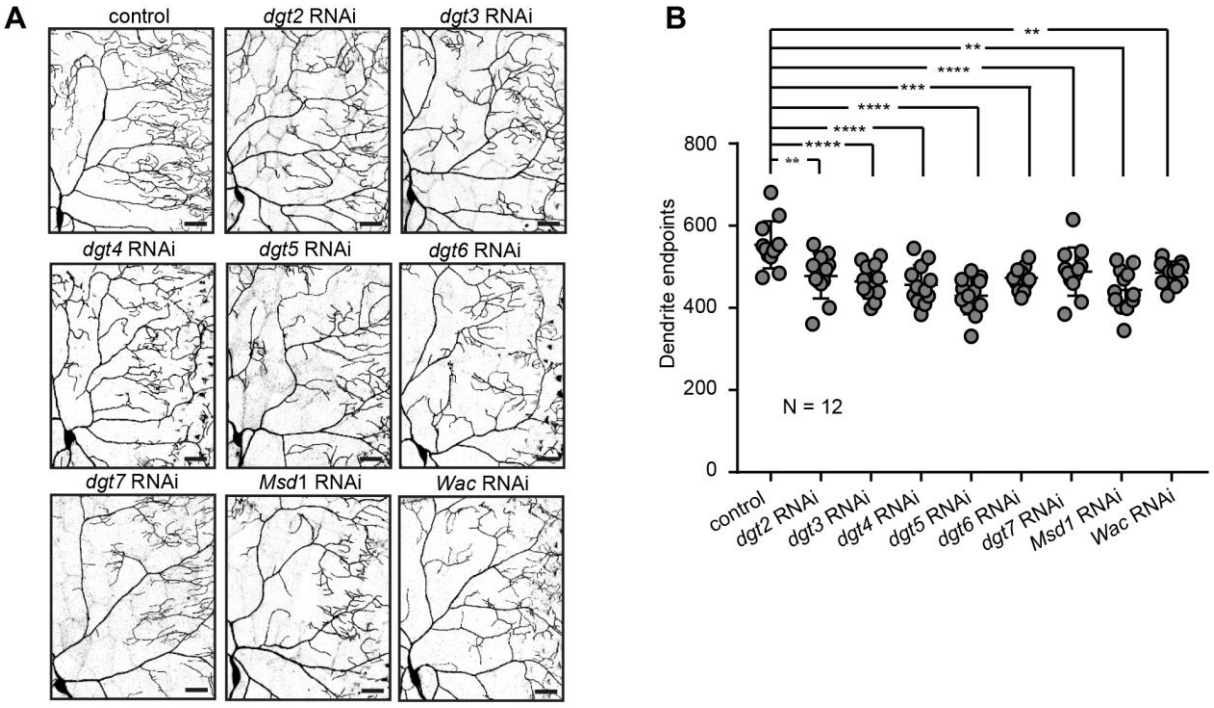

Fig. 4. All augmin complex subunits are required to establish a complex dendrite morphology. (A-B) Individual *Drosophila* augmin complex subunits were knocked down in c4da neurons of wandering LIII larvae. **(A)** One quadrant of individual c4da neurons is shown per genotype. **(B)** The number of dendrite endpoints was reduced upon the knockdown of each Augmin complex subunit. Statistical test used in B: 1-Way-ANOVA with Dunnett´s *post hoc* test. Scale bars = 50 µm.

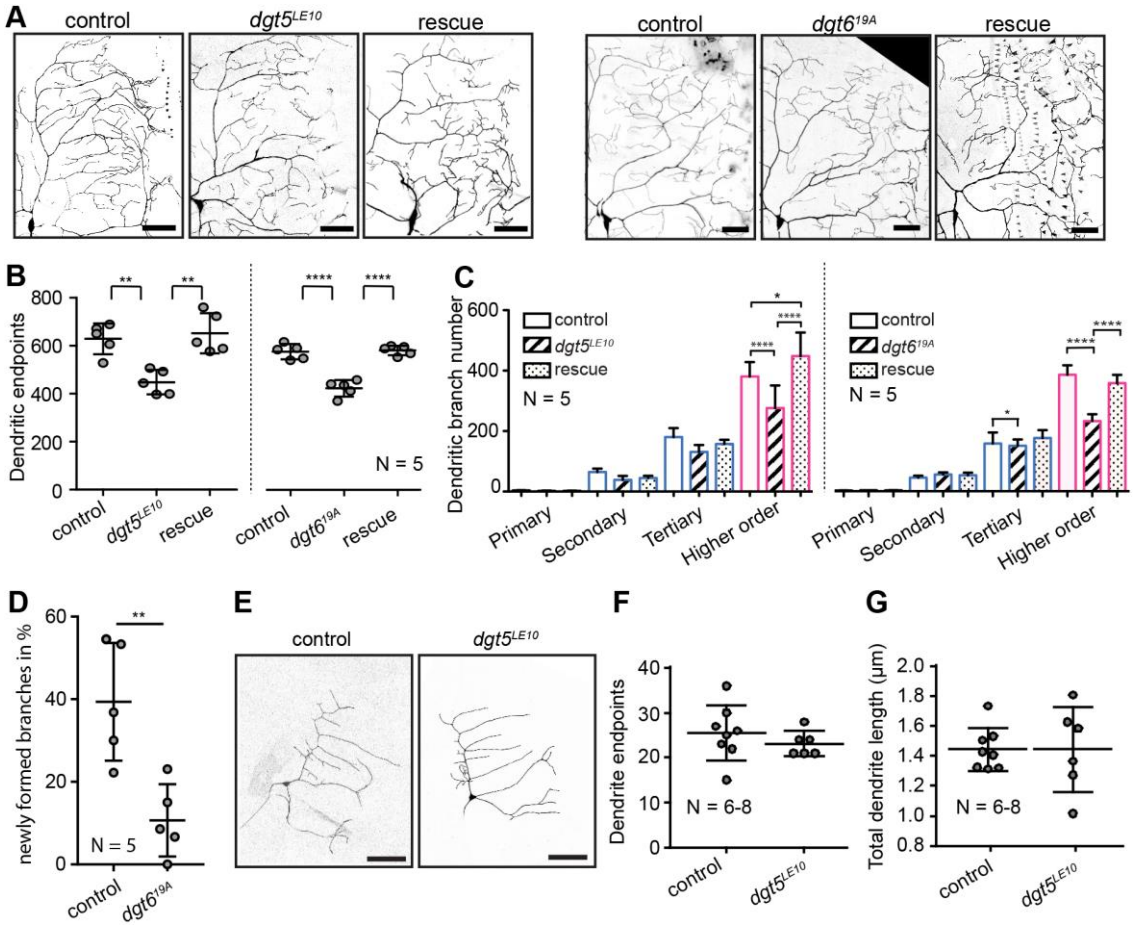

Fig. 5. Dgt5 and Dgt6 regulate terminal dendrite abundance *in vivo* in *Drosophila* c4da neurons. (A-C) Homozygous mutant *dgt5*^{LE10} c4da neurons and mutant *dgt5*^{LE10} c4da neurons expressing *UAS-dgt5* (rescue) were obtained in wandering LIII stage using MARCM (Lee and Luo 2001). C4da neurons were labeled using *Gal4*^{477} > *UAS-mCD8::GFP* in wandering LIII larvae, homozygous *dgt6*^{19A} mutant animals, or *dgt6*^{19A} mutants in which *UAS-dgt6* was re-expressed in c4da neurons (rescue). **(A)** Representative images of a quadrant of the full dendrite tree. **(B)** Quantifications of neuronal dendritic endpoints. **(C)** Dendritic branch numbers sorted by branch order. **(D)** The amount of newly formed branches was measured by *in vivo* time-lapse imaging in control and *dgt6*^{19A} mutant neurons at the LII stage. Images were acquired every 5 min for 30 min. **(E)** c1da control or *dgt5*^{LE10} mutant MARCM clones and quantification of their total dendrite length **(F)** as well as the number of dendrite endpoints **(G)**. Scale bars = 50 µm. Statistical tests used in B: 1-Way-ANOVA followed by Tukey's multiple comparisons test; in C: 2-Way-ANOVA followed by Tukey's multiple comparisons test; in D, F and G: unpaired student´s *t*-test. N = number of neurons analyzed.

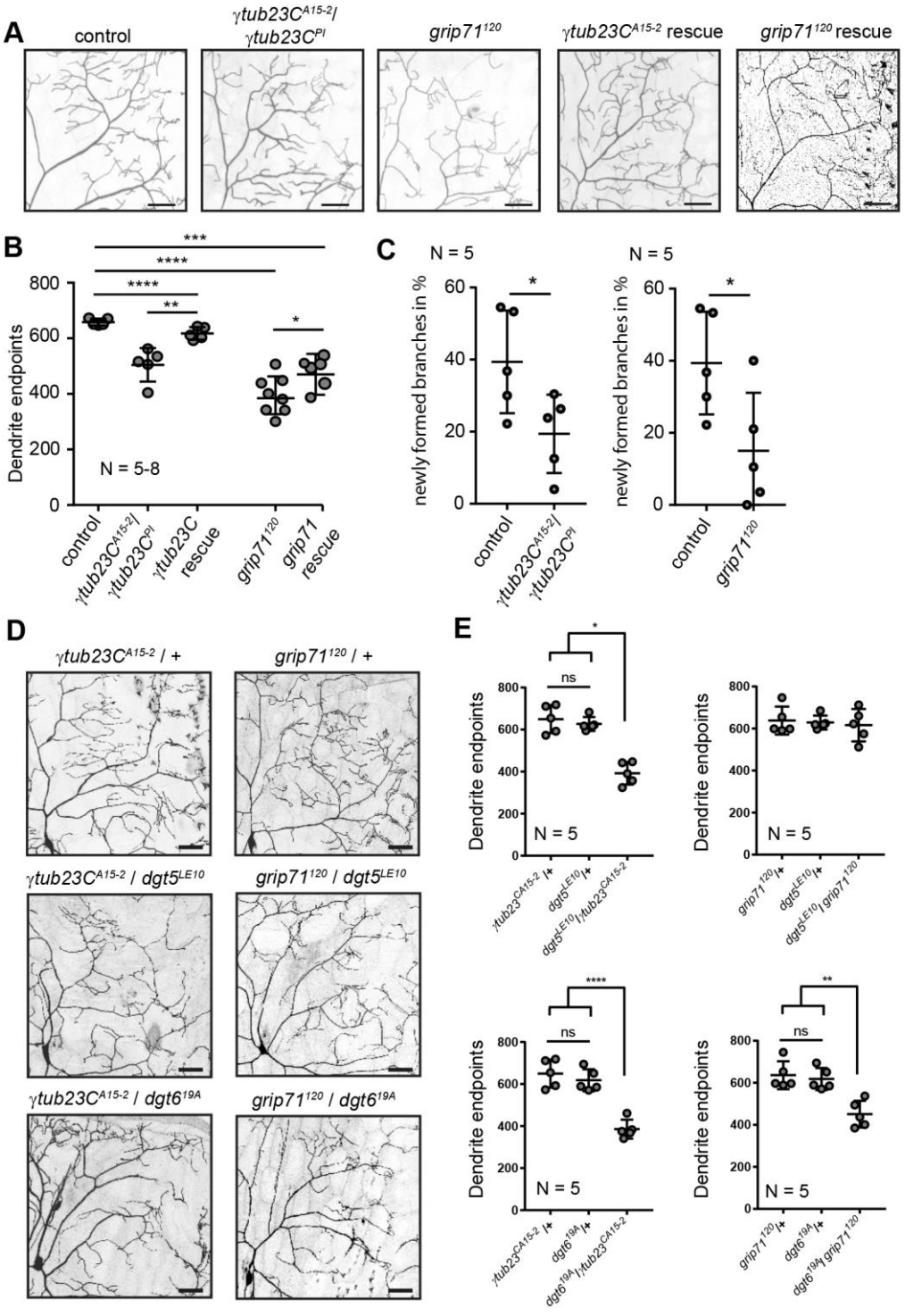

Fig. 6. γ-**TuRC and augmin complexes functionally cooperate during dendrite development. (A)** Representative confocal stack images of c4da neurons of a control genotype and the trans-allelic γ*tub23C*$^{A15-2}$/γ*tub23C*^{Pl} or *grip71*^{120} mutant at wandering LIII stage. Rescue experiments were performed by expression of either *UAS*-γ*tub23C::GFP* or *UAS-grip71::GFP* in c4da neurons using ppk-Gal4 in the respective mutant background. Scale bar = 50 µm. **(B)** The number of total dendritic endpoints was reduced in γ*tub23C* or *grip71*^{120} mutant c4da neurons and could be

cell-autonomously rescued. **(C)** The amount of newly formed branches was measured by *in vivo* time-lapse imaging in control, γ*tub23C* or *grip71*^{120} mutant c4da neurons at the LII stage. Images were acquired every 5 min for 30 min. **(D)** C4da neurons of heterozygous γ*tub23C*$^{A15\text{-}2}$/+, *grip71*^{120}/+ larvae or of trans-heterozygous combinations of these γ-TuRC components with heterozygous *dgt5* or *dgt6* mutants. **(E)** Quantification of total dendritic endpoints reveals a reduction in *dgt5*^{LE10}/γ*tub23C*$^{A15\text{-}2}$, *dgt6*^{19A} /γ*tub23C*$^{A15\text{-}2}$, *and dgt6*^{19A} */grip71*^{120} trans-heterozygous cells but not in the *dgt*^{5LE10}*/grip71*^{120} trans-allelic combination compared to single heterozygous mutants. Scale bar = 50 µm. Statistics in B: 1-Way-ANOVA with Turkey´s *post hoc* test, in C: Kruskal-Wallis with Dunn´s multiple correction test, in E: 1-Way-ANOVA with Turkey´s *post hoc* test.

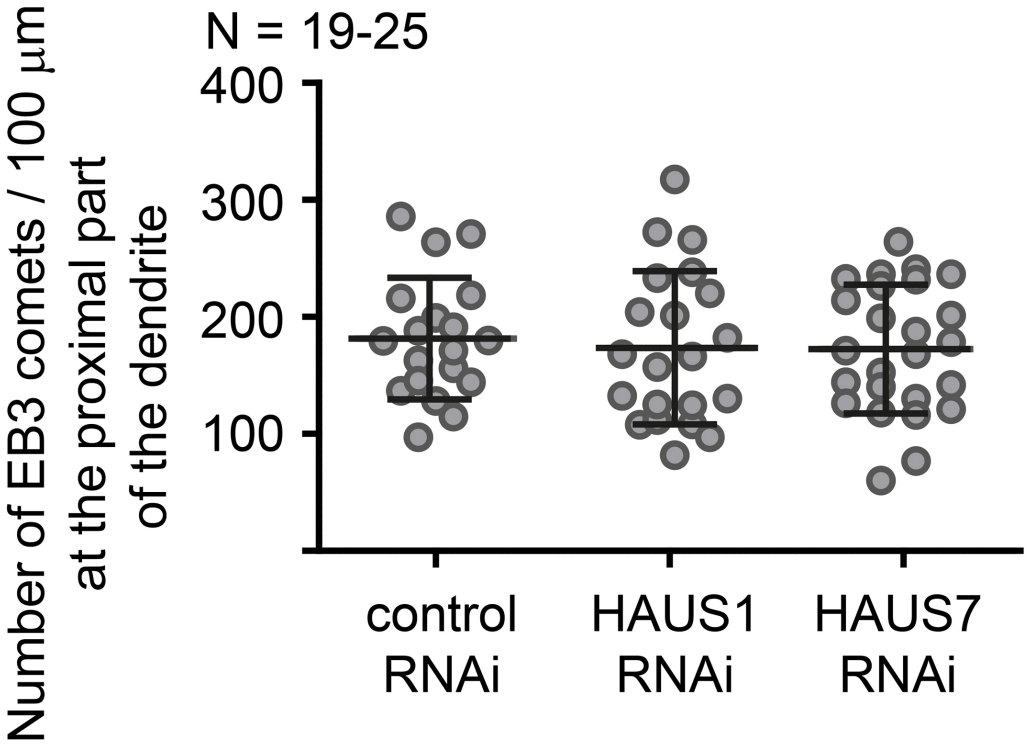

Fig. S1. Number of EB3 comets in proximal dendrites in cultured hippocampal neurons. The number of EB3 comets in primary hippocampal neurons cultures at DIV 5 was unchanged upon HAUS1 or HAUS7 depletion. Statistics: 1-Way-ANOVA with Turkey's *post hoc* test.

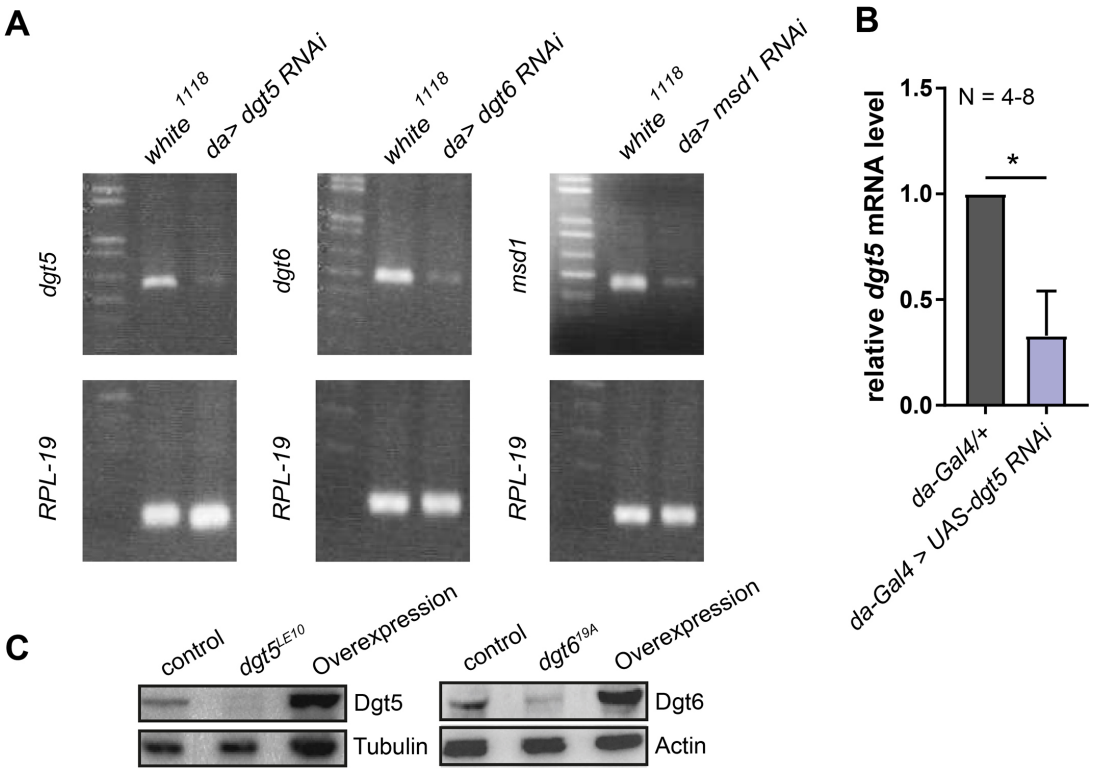

Fig. S2. (A) Knockdown efficiency of *dgt5*, *dgt6* and *msd1* RNAi constructs. Knockdown efficiency was tested by driving the respective UAS-ds RNA construct broadly using daugthterless (da)-Gal4. mRNA was obtained from LIII larvae and amplification of *ribosomal protein L19* (*RPL-19*) was used as control. **(B)** *da-Gal4* was used to drive to test the knockdown efficiency of the *dgt5* RNAi construct. Animals were raised at 27°C. N represents the number of biological replicates. Statistical test used: Mann-Whitney test. **(C)** Western blots loaded with total protein extracts of 20 homozygous mutant embryos (left panel) or five third instar larvae (right panel) and probed with anti-Dgt5/anti-Dgt6 antibodies. α-Tub labeling served as loading control. Dgt5 protein is not detectable in extracts of homozygous $dgt5^{LE10}$ embryos; Dgt6 protein levels are drastically reduced in extracts of homozygote $dgt6^{19A}$ mutant LIII larvae. Dgt5 and Dgt6 signals could be restored by *krüppel-Gal4*-driven expression of *UAS-dgt5* or *UAS-dgt6* in the respective mutants (rescue).

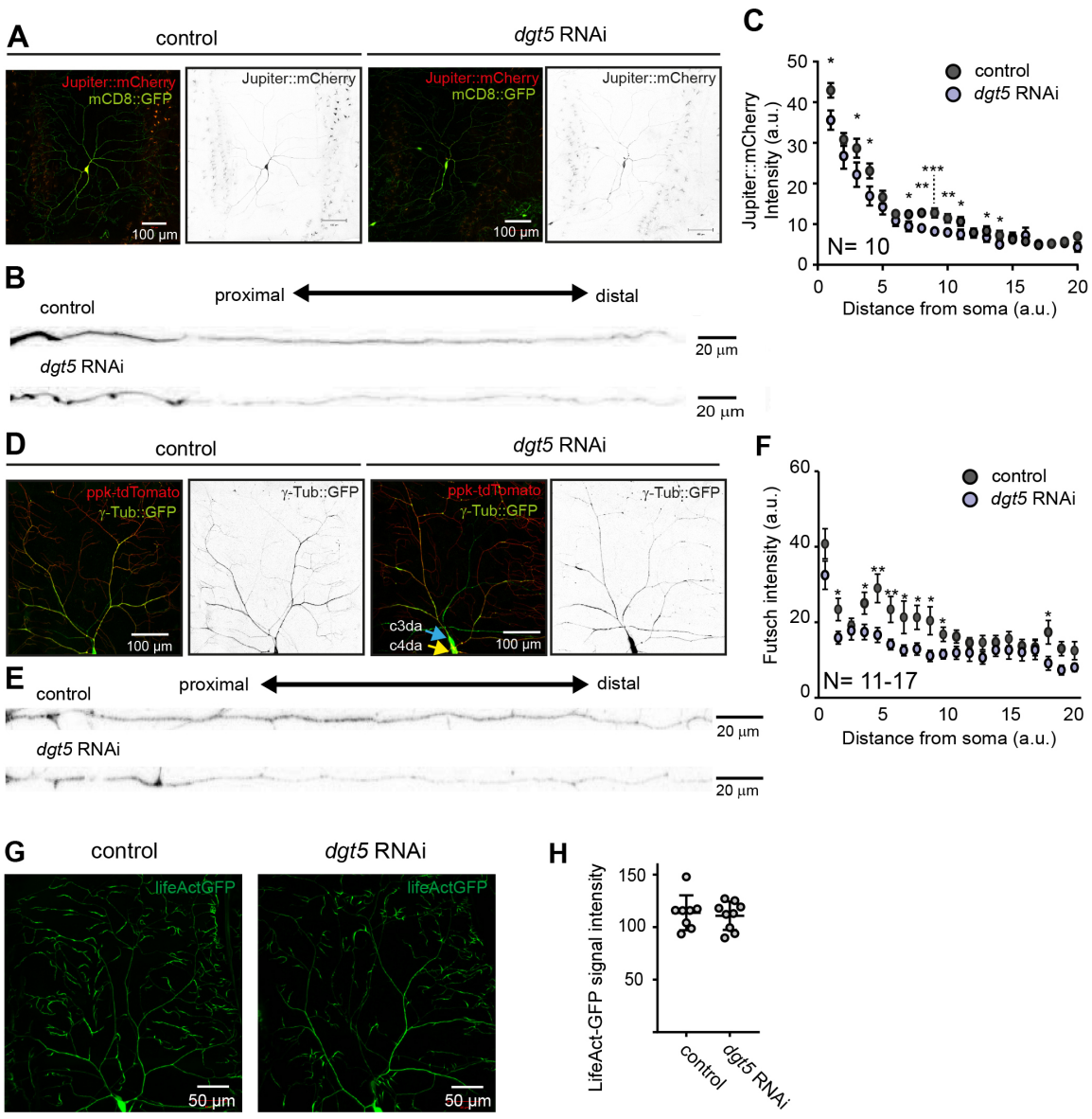

Fig. S3. Dgt5 modulates MT but not actin density. (A-C) C4da neurons expressing the MT marker Jupiter::mCherry and the membrane-associated mCD8::GFP under the control of *ppk-Gal4*. Simultaneously, a control (UAS-lacZ) or a *UAS-dgt5* RNAi construct were co-expressed. **(A)** Representative confocal images. **(B)** Jupiter::mCherry signal along individual dendrites. **(C)** Quantified Jupiter::mCherry signal intensity levels in *dgt5* knockdown and control dendrites**. (D-E)** Control or *dgt5* knockdown c4da neurons labeled by *ppk-tdTomato* expression. Simultaneously-expressed γ-Tub::GFP . **(D)** Representative confocal images. **(E)** γ-Tub::GFP signal along individual dendrites. **(F)** Quantified γ-Tub::GFP signal intensity levels in *dgt5* knockdown and control dendrites**. (G-H)** *UAS-lifeAct* expression was driven by ppk-Gal4 in *dgt5* knockdown and control c4da neurons **(G)** Representative confocal images. **(H)** Quantified LifeAct::GFP levels. Statistics in C, F and H: two tailed student´s *t*-test.

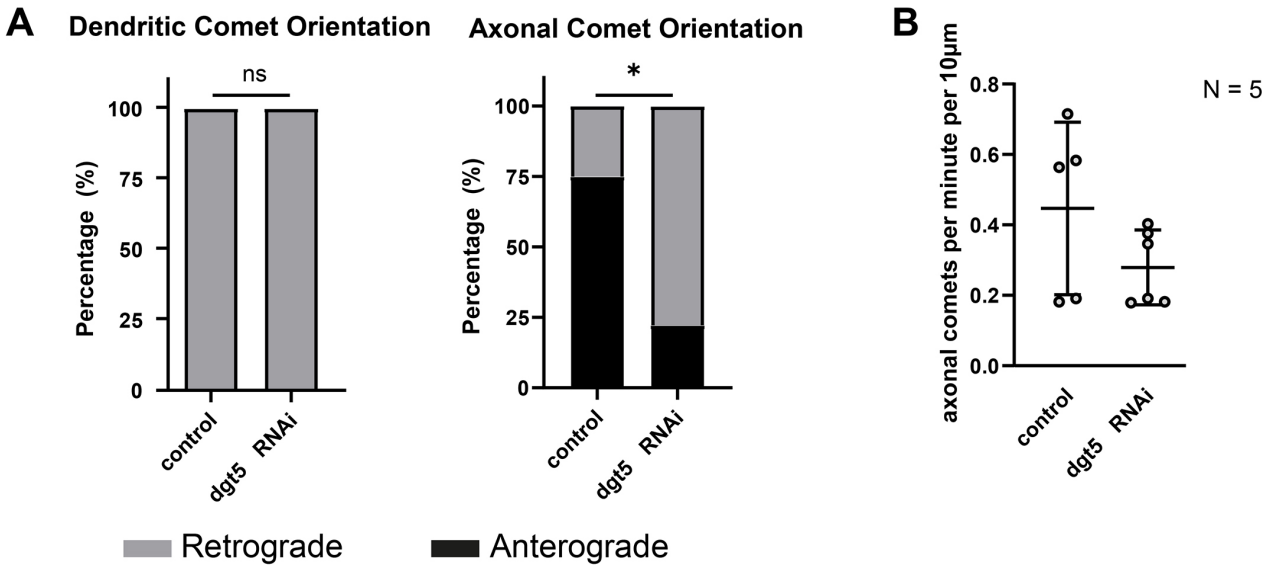

Fig. S4. Dgt5 knockdown affects axonal but not dendritic MT orientation. *ppk*-EB1::GFP comets were imaged in control or dgt5 depleted c4da neurites. **(A-B)** dgt5 RNAi-knockdown affects axonal **(A)** but not dendritic **(B)** MT orientation. **(C)** EB1::GFP comet number was not affected in axons. Statistical test used in C: two-tailed Students *t*-test.

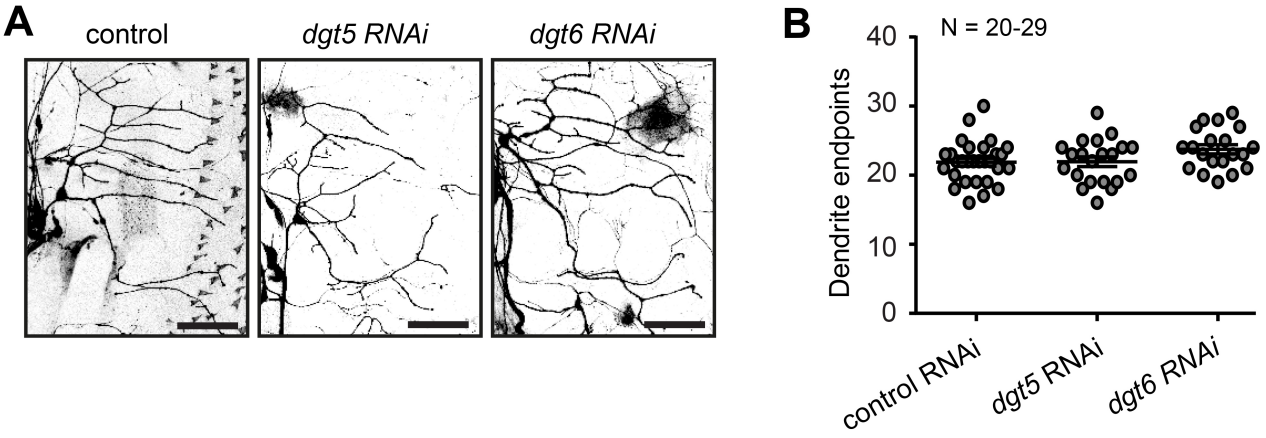

Fig. S5. Reduction of augmin function does not modify c1da dendrite complexity. *UAS-dgt5 RNAi, UAS-dgt6* or a control construct were expressed together with *UAS-mCD8::GFP* under the control of the c1da neuron driver. The number of dendrite endpoints is not modified upon knockdown of *dgt5* or *dgt6*. Scale bars = 50 µm. Statistical test: 1-Way-ANOVA + Dunnett´s *post hoc* test.

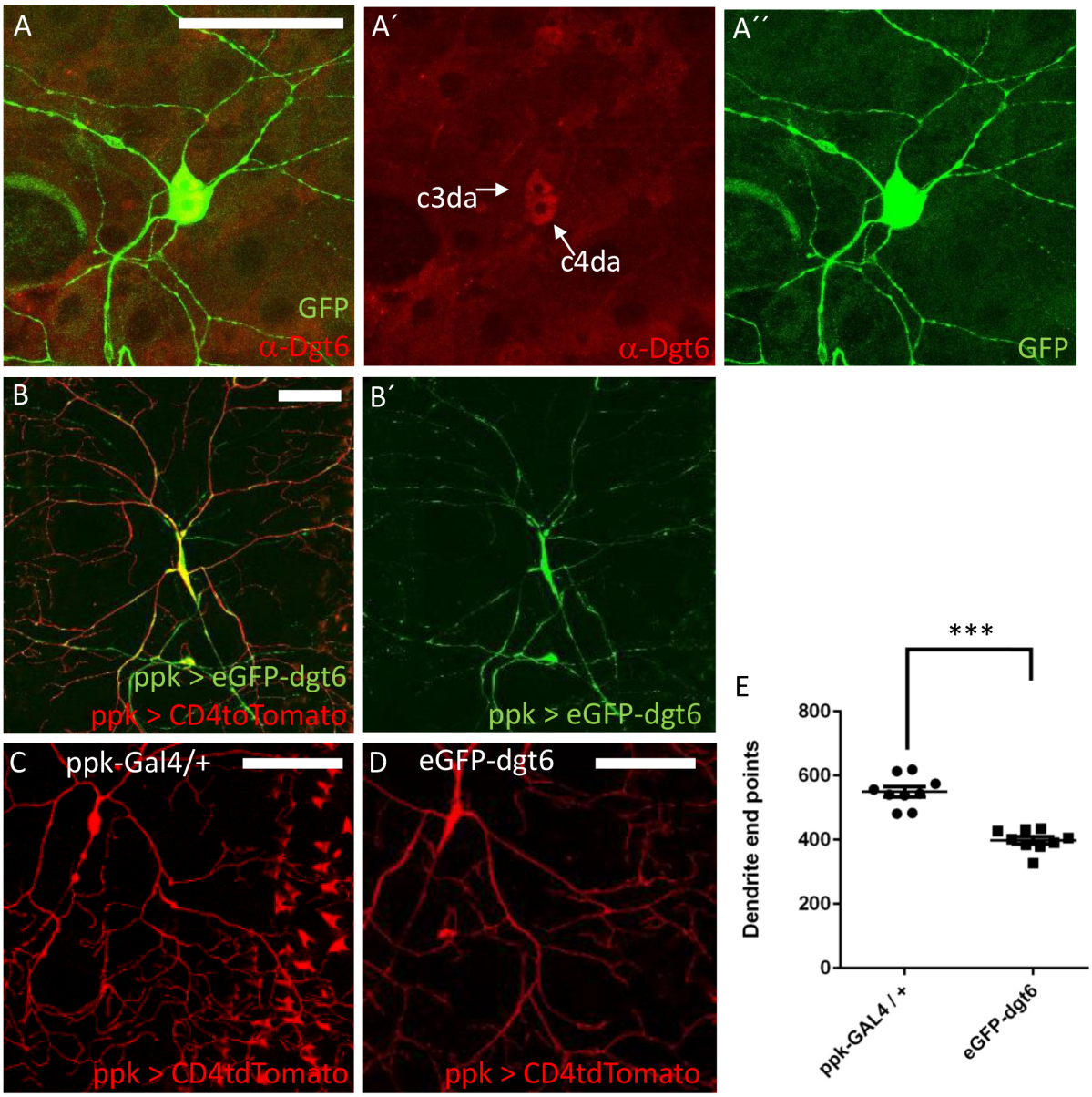

Fig. S6. Dgt6 localization in c4da neurons. (A) Anti-Dgt6 labeling (red) in c4da and c3da neuron labeled by *ppk-Gal4* driven expression of *UAS-mCD8::GFP* (green). **(B-D)** *ppk-Gal4* driven expression of *UAS-CD4tdTomato* was used to label c4da neurons and to simultaneously express *eGFP-dgt6* **(B, D). (E)** The number of dendrite endpoints was reduced upon the expression of *eGFP-dgt6*. Statistical test used in B: two-tailed Students *t*-test. Scale bars = 100 µm.